A TNL receptor mediates microbiome feedbacks in Arabidopsis

Authors:

Henry Janse van Rensburg[1*], Niklas Schandry[2,3*§], Jan Waelchli[1], Katja Stengele[1], Selma Cadot[1], Katharina Jandrasits[2], Claude Becker[2,3,§], Klaus Schlaeppi[1,§]

[1] Department of Environmental Sciences, University of Basel, Basel, Switzerland

[2] Gregor Mendel Institute of Molecular Plant Biology GmbH, Austrian Academy of Sciences, Vienna BioCenter (VBC), Vienna, Austria

[3] LMU Biocenter, Faculty of Biology, Ludwig-Maximilians-Universität Munich, Martinsried, Germany

[*] Contributed equally

[§] **Corresponding authors:**

Niklas Schandry: n.schandry@bio.lmu.de

Claude Becker: claude.becker@lmu.de

Klaus Schlaeppi: klaus.schlaeppi@unibas.ch

ORCID identifiers:

H. J.v.R.:	0000-0002-5632-8422
N. S.:	0000-0003-3099-7860
K. St.:	0009-0008-3843-2868
J. W.:	0000-0002-4384-6570
K. J.:	0000-0002-0161-582X
C. B.:	0000-0003-3406-4670
K. S.:	0000-0003-3620-0875

Author contributions:

H.J.v.R., N.S., C.B., and K.S., designed the research; H.J.v.R. and K. St. performed greenhouse and S.C. the field soil conditionings; K.J and N.S. performed the phenotyping of accessions and GWA analysis; H.J.v.R. performed GWA candidate gene selection, MBOA sensitivity assays, genetic characterisation of Arabidopsis mutants, Arabidopsis mutant feedback, microbiome and transcriptome experiments and analysis; J.W., performed bioinformatic analysis for the microbiome and transcriptome analyses; C.B., provided funding and access to high-throughput phenotyping infrastructure; H.J.v.R. and N.S. analysed the data; H.J.v.R., N.S. and K.S. wrote the manuscript. All authors revised the paper.

Manuscript information:

Number of Figures: 5 (all colour)

Number of Supplementary Materials figures: 9

Number of Supplementary Materials tables: 3

Declarations of interest:

none

Abstract

Plant performance depends on the soil microbiome. While microbiome feedbacks are well documented, the mechanisms by which plants perceive and mediate these feedbacks remain unclear. We established a framework using two distinct microbiomes in the same soil that differently affect plant growth. Screening 410 *Arabidopsis thaliana* accessions revealed substantial variation in growth feedbacks, which we used for genome-wide association mapping to identify Mediator of Microbiome Feedback 1 (MMF1), an immune receptor. Characterisation in the reference accession Col-0 revealed that *mmf1* mutants lack the differential growth feedbacks, have an altered root bacterial community, and fail to induce a defence-related transcriptional response observed in wild-type plants. The discovery of MMF1 implies that integration of microbial effector signals optimises host microbiome composition and immune status to enhance growth.

Keywords

Growth feedback, GWAS, Arabidopsis, soil microbiome, TNL receptors

59 **Main**

60 Microbiomes are widely recognized for supporting their hosts with many vital services leading to
61 improved host performance. Similar to the gut microbiome of humans, plant microbiomes contribute to
62 nutrition homeostasis, stress tolerance and host health (*1*). A large knowledge gap in all fields of host-
63 microbiome interactions, is how hosts genetically control their microbiome. For plants, the performance
64 depends to a large extent on below-ground bacteria, fungi and other microbes that collectively function
65 as a soil microbiome (*1*, *2*). Soil microbiomes consist of functionally diverse members providing
66 beneficial services to plants, including nutrient acquisition, growth promotion, stress tolerance, and
67 suppression of plant pathogens, but soil microbiomes can also contain pathogenic members that reduce
68 plant fitness (*3*, *4*). Plant responses, which are causally linked to a soil microbiome, are referred to as
69 microbiome feedbacks (*5*). This term is akin to plant-soil feedbacks describing the ecology of soil
70 properties (more broadly, but including the microbiome) that influence plant performance (*6*, *7*).
71 Microbiome feedbacks are highly relevant in agricultural contexts, as soil microbiome composition has
72 been linked to agronomic traits of crops such as maize and potato (*8*, *9*), to field productivity (*10*), and
73 to over- and under yielding areas in fields (*11*, *12*). While different soil microbiomes have often been
74 seen as drivers of differential plant responses (*13*, *14*), little is known about the mechanisms by which
75 plants perceive complex soil microbiomes and mediate microbiome feedbacks.

76 Plants have evolved a sophisticated immune system that regulates interactions with beneficial
77 microbes while defending against pathogens (*15–17*). Plant immunity operates through two key
78 pathways: pattern-triggered immunity (PTI) and effector-triggered immunity (ETI). PTI is initiated at
79 the cell surface by pattern-recognition receptors that recognize microbe-associated molecular patterns
80 and provides basal defence to deter non-adapted microbes. In contrast, ETI is activated within the
81 cytoplasm by nucleotide-binding leucine-rich repeat receptors (NLRs), which detect pathogen effectors
82 or their activities, leading to definite immune responses (*18–20*). NLRs are divided into
83 Toll/interleukin-1 receptor (TIR-NLRs; TNLs) and coiled-coil NLRs (CNLs). *Arabidopsis thaliana*
84 (hereafter: Arabidopsis) encodes 54 TNLs and 88 CNLs, highlighting the complexity of the plant
85 immune system (*21*). Both PTI and ETI depend on signalling molecules such as salicylic acid (SA) and
86 reactive oxygen species (ROS) (*19*, *20*). Although these pathways were primarily studied in the context
87 of binary interactions with pathogenic or beneficial microbes, recent evidence suggests that PTI and
88 ETI also influence plant-associated microbiomes. These immune pathways shape microbiome
89 composition, modulating microbial interactions and contributing to overall plant health and resilience
90 (*16*, *22–24*).

91 To study microbiome feedbacks, we developed an experimental framework based on two
92 distinct soil microbiomes in the same soil type. These soil microbiomes are generated by growing wild-
93 type maize, which produces benzoxazinoids (BXs), or BX-deficient mutant maize. BXs are bioactive
94 compounds of *Poaceae* (*25*) that, among multiple functions, shape the root and rhizosphere
95 microbiomes of plants (*14*, *26*, *27*). After three months of growth, the wild-type and mutant plants are

removed, leaving behind BX-conditioned (BX_{plus}) and its control (BX_{minus}) soil microbiomes, respectively. We have described growth and defence feedbacks of maize and wheat in response to BX_{minus} and BX_{plus} soil microbiomes (*14*, *28*), and we have proven agronomic relevance of these microbiome feedbacks (*28*, *29*). Through sterilization and microbiome complementation experiments, we demonstrated that the feedbacks are BX-dependent but that the soil microbiomes drive the differential plant responses (*14*, *28*, *29*). Recently, we found that the model plant Arabidopsis also expressed microbiome feedbacks (*30*). The reference accession Columbia-0 (Col-0) responded with improved growth and enhanced resistance when grown on the BX_{plus} compared to the BX_{minus} soil microbiome. As plausible mechanistic explanation for this apparent lack of a growth-defence trade-off, the plants growing on the BX_{plus} soil microbiome were found to be primed for their SA defences (*31*). Microbiome feedbacks are often influenced by the genotype of the response plant. For instance, rhizobacteria-induced growth promotion varied significantly across Arabidopsis accessions (*32*). Similarly, genotype-specific resistance against Fusarium has been observed in tomato, where the outcome of the interaction depends on the tomato genotype and the composition of the native soil microbiome (*13*). In our work with maize and wheat responding to BX_{minus} and BX_{plus} soil microbiomes, we also observed a genetic component in microbiome feedbacks (*14*, *28*). Here, we harnessed the genetic diversity among Arabidopsis accessions to study their growth feedbacks as a function of the plant genotype and the soil microbiome (**fig. S1**).

115 **Results**

116

117 ***Arabidopsis displays substantial phenotypic variation in microbiome feedbacks***

118 We grew 410 natural, genome-sequenced Arabidopsis accessions (*33*) in both control (BX_{minus}) and BX-
119 conditioned (BX_{plus}) soil microbiomes in a climate chamber equipped with an automated top-view
120 imaging system. The process from imaging to determination of rosette area and feedback calculation is
121 illustrated with the two contrasting accessions IP-Hue-3 and Hadd-3, which grew better and worse on
122 the BX_{plus} soil microbiome, respectively (**Fig. 1ab**). Plants were imaged twice a day and plant
123 morphometric traits extracted using ARADEEPOPSIS (*34*). We focussed on the first 20 days after
124 germination (DAG) to avoid confounding phenotyping effects such as early flowering and overlapping
125 leaves. We used rosette area as a measurement of plant size to calculate the daily growth feedback as
126 the difference in rosette area between BX_{plus} and BX_{minus} microbiomes, i.e. the accessions IP-Hue-3 and
127 Hadd-3 exhibited positive and negative feedbacks, respectively (**Fig. 1b**).

128 The screening of accessions revealed substantial variation in growth feedbacks to BX_{plus} and
129 BX_{minus} microbiomes (**Fig. 1c; Dataset 1** and **Suppl. File 1**). Across the 410 accessions, 48 % (196
130 accessions) displayed positive feedbacks, while 52 % (214 accessions) showed negative feedbacks. At
131 the two extremes of the distribution, the two soil microbiomes accounted for ~2-fold (IP-Hue-3) and
132 >3-fold (Hadd-3) differences in rosette area. Consistent with earlier work, Col-0 expressed a subtle
133 positive feedback (*30*). Feedback responses were independent of the accessions' geographical origin
134 (**Fig. 1d, fig. S2a**).

135 Since BXs are allelopathic to plants (*35*, *36*), we tested whether the accession's growth
136 differences could be due to varying sensitivity to BXs. BXs differ between the two soil variants, with
137 MBOA as the most abundant BX compound (*29*, *37*). We screened the subset of accessions with the
138 strongest opposing growth feedbacks for sensitivity to MBOA. All accessions exhibited shorter roots
139 in the presence of MBOA (**fig. S3a, Dataset 2** and **Suppl. File 2**), which is indicative of phytotoxicity.
140 However, there was no correlation between feedback response and MBOA sensitivity (**fig. S3b**). These
141 results indicate that the observed growth feedbacks are not linked to varying sensitivity to the BXs
142 present in the soil.

143 In conclusion, we found substantial phenotypic variation in Arabidopsis growth feedbacks to
144 two soil microbiomes, providing a powerful resource for association studies on genetics that drive the
145 differences in feedbacks.

146

147

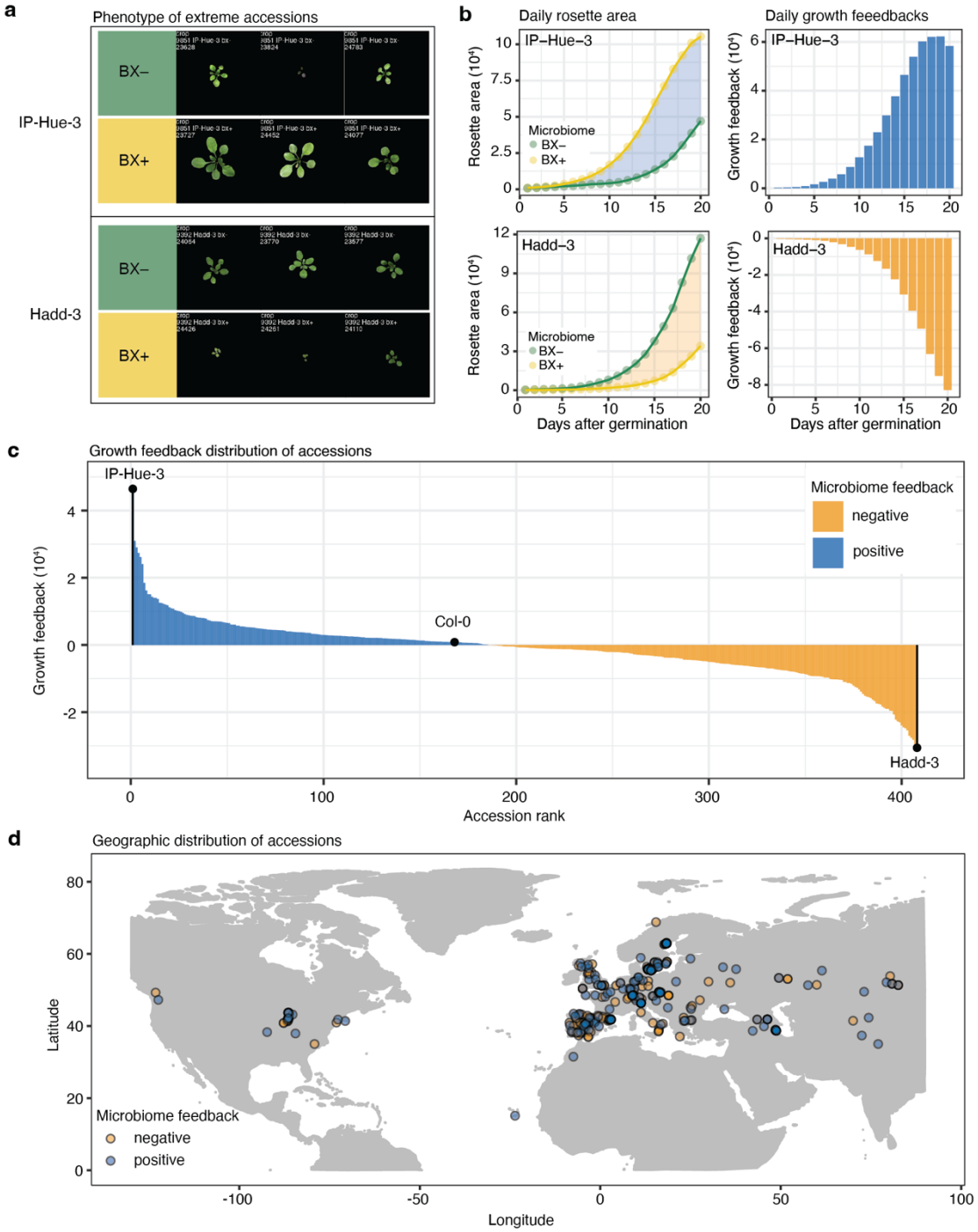

Figure 1. **Natural variation in growth feedbacks among Arabidopsis accessions**. (**a**) Growth of the two *A. thaliana* accessions (IP-Hue-3 and Hadd-3) that exhibited the largest opposing growth feedbacks in response to the BX_{minus} and BX_{plus} microbiome at the conclusion of the experiment (20 days after germination (DAG)). (**b**) The daily rosette area measured in pixels extracted by ARADEEPOPSIS (left), and the daily microbiome growth feedback (BX_{plus} – BX_{minus}) (right) for the first 20 DAGs for IP-Hue-3 and Hadd-3 grown on the two soil microbiomes. Shaded areas (left) and coloured bars (right) indicate positive (blue, IP-Hue-3) or negative (orange, Hadd-3) microbiome feedbacks in response to the BX_{plus} microbiome. (**c**) Microbiome feedback of the 410 *A. thaliana* accessions used in the genome-wide association study at the conclusion (DAG 20) of the experiment. The position of IP-Hue-3, Hadd-3 and Col-0 are indicated on the graph. Data is from two phenotyping experiments (experiment I and II, **Table S1**), each consisting of a subset of 210 accessions (3 replicates per accessions per soil), with 10 overlapping accessions in each of the experiments. (**d**) The map shows the geographic distribution of these accessions, coloured by their microbiome feedback (blue for positive; orange for negative).

160 ***Candidate gene loci are involved in plant growth and defence***

161 We performed a genome-wide association study (GWAS) using the phenotypic variation in growth
162 feedbacks of the 410 accessions (**Fig. 1c**) and employed a linear mixed model accounting for population
163 structure among the used Arabidopsis accessions (*38*). Noting temporal variation in daily growth
164 feedbacks (**fig. S2b**), we ran separate GWAS on daily data, and calculated associations between single
165 nucleotide polymorphisms (SNPs) and the phenotypes for each of the 20 DAGs (**Dataset 3)**.

166 Across daily GWAS runs, we identified three genomic regions with significant associations to
167 the growth feedback (**Fig. 2a; Dataset 3** and **Suppl. File 3**). Genes in the regions of the three peaks are
168 related to plant growth and plant defence. We then focused on SNPs that were significant for multiple
169 consecutive days in the repeated GWAS (see Methods). The top SNP (chromosome 3, position
170 16203882) was in peak #2 (**Fig. 2b**), of which an alternative allele was found in 11 accessions (**Fig.
171 2c,d**). These accessions expressed better growth in response to the BX_{plus} microbiome compared to
172 accessions with the reference allele of the SNP (**Fig. 2c**). This SNP is in close proximity to the TNL
173 receptor gene AT3G44630 (position 16200156; 3.7kb upstream) and a more distal second TNL
174 (AT3G44670; position 16218427; 14.5kb downstream; **Fig. 2b**). We focussed on the uncharacterized
175 AT3G44630 because of the closer proximity to the top SNP, and its differential expression in roots of
176 Arabidopsis grown on BX_{minus} and BX_{plus} soils (*30*). We named this gene *Mediator of Microbiome*
177 *Feedback 1* (*MMF1*). Taken together, GWAS identified a genomic locus on chromosome 3 that includes
178 *MMF1* as a candidate gene that could explain the differential growth feedbacks of Arabidopsis
179 accessions in response to the BX microbiomes.

180

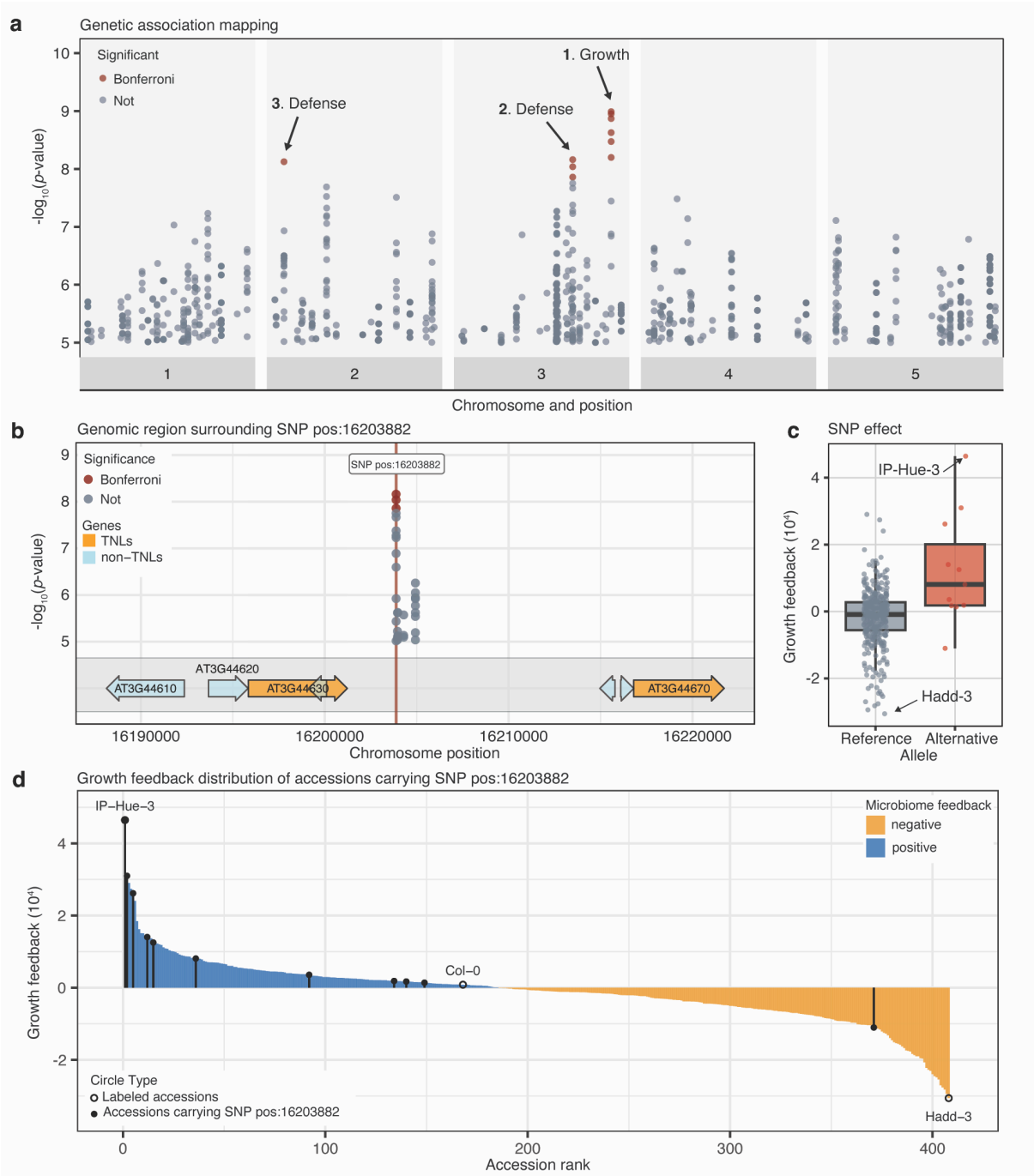

Figure 2. Genetic association mapping of growth feedbacks in response to the BX_{plus} microbiome. (**a**) Manhattan plot showing the -$\log_{10}$-transformed *p*-values for the top 500 single nucleotide polymorphisms (SNPs) across the 5 chromosomes of *A. thaliana*. SNPs that are significantly associated with growth feedbacks after Bonferroni correction are shown in red. The biological functions of genes adjacent to the top three SNPs are indicated. (**b**) The genomic region (50 kb) flanking the SNP at position 16,203,882, including the two TNL genes AT3G44630 and AT3G44670. (**c**) Average growth feedback among accessions carrying the alternative allele of the SNP at position 16,203,882 (positive feedback) compared to those with the reference allele (negative feedback). (**d**) Overall positive microbiome feedback distribution of accessions carrying the alternative allele of the SNP at position 16,203,882 (black lines and filled circles) on the growth feedback distribution curve at the conclusion of the experiment.

194 ***MMF1 mediates differential microbiome feedbacks***

195 To test if MMF1 functions in growth feedbacks, we phenotyped two T-DNA insertion lines in the Col-
196 0 background for their response to the BX_{minus} and BX_{plus} microbiomes. The *mmf1-1* and *mmf1-2* lines
197 are knockdown and knockout mutants, respectively (**fig. S4**). Both mutants grew similarly to wild type,
198 albeit slightly smaller, and showed no obvious disease symptoms (**Fig. 3a; Dataset 4** and **Suppl. File**
199 **4**). Consistent with earlier work (*30*) and the GWAS experiment (**Fig. 1c**), wild- type plants expressed
200 subtle positive growth feedbacks in response to the BX_{plus} microbiome, with higher fresh weight and
201 larger rosette area compared to those growing on the BX_{minus} microbiome (**Fig. 3b**).

202

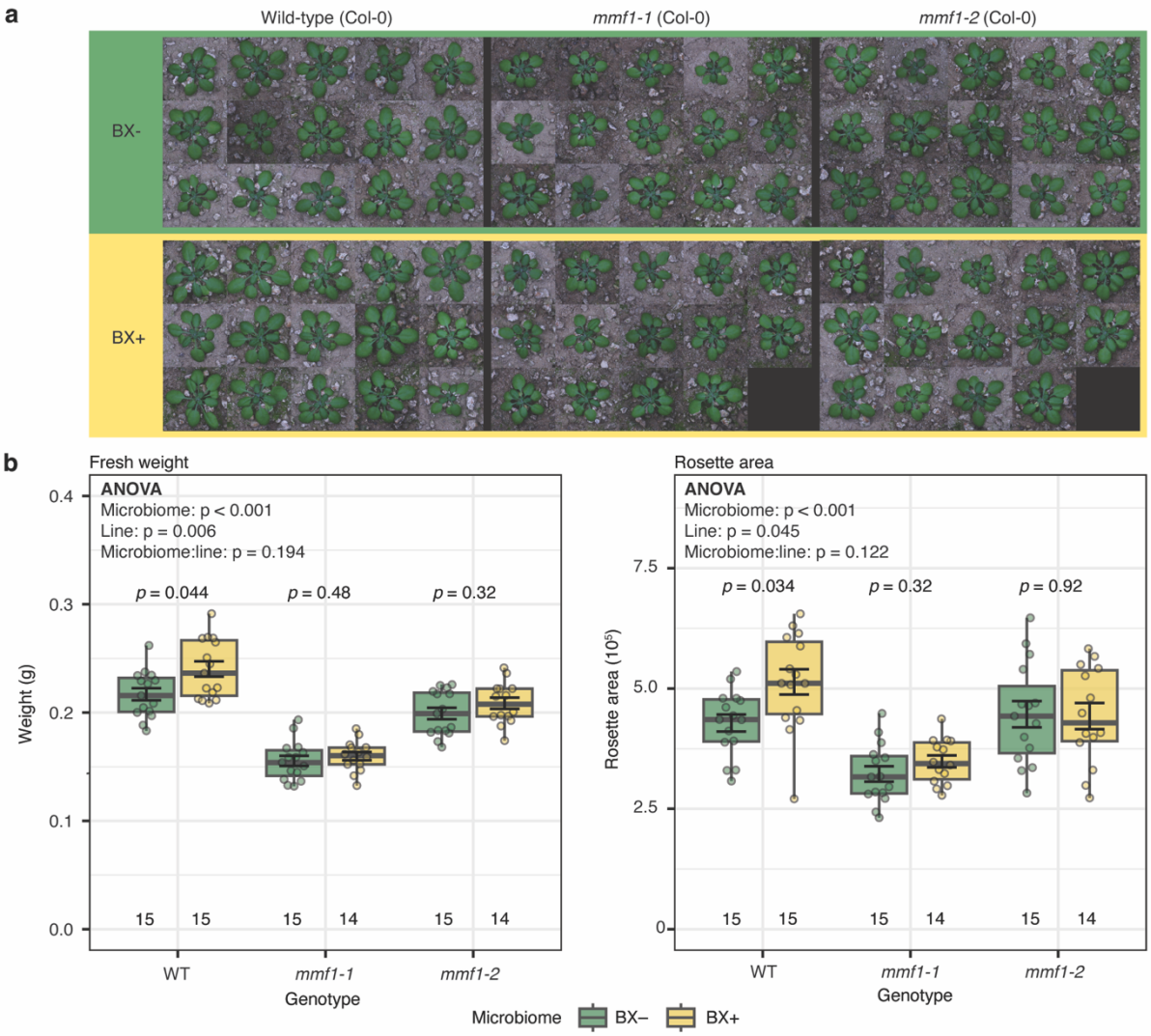

203

204 **Figure 3**. **MMF1 is involved in growth feedback responses to the BX_{plus} microbiome**. (**a**) Phenotypes of 6-
205 week-old Col-0 wild-type (WT) and two *mmf1* T-DNA insertion mutants (AT3G44630) grown on the BX_{minus} and
206 BX_{plus} soil microbiomes (experiment IV, **Table S1**). (**b**) Fresh weight (left) and rosette area (right; in pixels) of
207 the indicated genotypes grown for 6 weeks on either a BX_{minus} or BX_{plus} microbiome. Sample sizes are indicated
208 at the bottom of each plot. Boxplots illustrate the median, standard error, and interquartile range, and the whiskers
209 extend from the box to the smallest and largest values. Output of the ANOVA and the FDR corrected *p*-values
210 are indicated in each plot. Results were confirmed in three independent repetition experiments (experiment III, IV
211 and V) on two independently conditioned soil batches.

212 In contrast, both *mmf1* mutants lost the positive growth feedback, reflected in fresh weight and rosette
213 area. This was confirmed in two additional experiments using independent soil batches (**fig. S5a,b**).
214 This functional validation allowed to conclude that, in Col-0, a functional MMF1 is required for the
215 differential growth feedback in response to the two soil microbiomes.
216 The plant immune system relies on two TNL signalling pathways: Enhanced Disease
217 Susceptibility 1 (EDS1) together with Phytoalexin Deficient 4 (PAD4) lead to resistance, and EDS1
218 jointly with Senescence-Associated Gene 101 (SAG101) induce hypersensitive responses and cell death
219 (*39*). To test the involvement of the two TNL signalling pathways in microbiome feedbacks, we
220 performed feedback assays with *eds1*, *pad4* and *sag101* mutant plants (*40*, *41*). These mutants showed
221 no altered growth phenotypes or obvious disease symptoms in response to BX_{minus} and BX_{plus} soil
222 microbiomes (**fig. S5c**). Similar to wild type, the three immune signalling mutants expressed positive
223 growth feedbacks in response to the BX_{plus} soil microbiome (**fig. S5d**). Hence, single gene knockouts
224 in EDS1, PAD4 and SAG101 do not disrupt immune signalling that leads to growth feedbacks, or
225 alternatively, suggest that this process may be independent of these two classical pathways.
226
227 ***MMF1 affects root bacterial community assembly sourced from BX_{plus} soil microbiome***
228 In earlier work, we found differential microbiomes on roots of plants with differential growth feedbacks
229 (*14*, *30*). We therefore determined the root bacterial, fungal and oomycete communities that wild-type
230 and *mmf1* mutant plants source from BX_{minus} and BX_{plus} soils. The detailed microbiome analysis is
231 documented in **Dataset 5** and **Suppl. File 5**. Shannon diversity did not differ between the factors
232 *microbiome* (BX_{minus} and BX_{plus}) and *line* (WT and *mmf1-2*; **fig. S6a**). We used Permutational
233 Multivariate Analysis of Variance (PERMANOVA) to assess the impact of these factors on root
234 community composition. *Microbiome* alone accounted for little variation in bacterial (R^2 = 3.9%, p =
235 0.09), fungal (R^2 = 3.7%, p = 0.25) and oomycete communities (R^2 = 5.5%, $p < 0.01$; **Fig. 4a**). However,
236 we found significant variation in bacterial – but not fungal or oomycete – communities between wild
237 type and *mmf1* mutants (R^2 = 5.7 %, $p < 0.01$) and in the interaction of the factors *line* with *microbiome*
238 (R^2 = 4.2 %, $p < 0.05$). The interaction effect indicates that the root microbiome of the mutant differed
239 from wild type in only one soil. Reduced pairwise PERMANOVA confirmed this with more and
240 significant variation between wild type and mutants in the BX_{plus} (R^2 = 15.7 %, $p < 0.01$) compared to
241 the BX_{minus} (R^2 = 4.6 %, p = 0.605) soil microbiome. In contrast, fungal and oomycete communities
242 showed no differences between *lines* and *microbiomes* (**fig. S6b**). Constrained Analysis of Principal
243 Coordinates (CAP) confirmed these findings: root bacterial communities clearly separated between
244 wild type and mutant on the BX_{plus} but not BX_{minus} soil microbiome (**Fig. 4b**), while fungal and
245 oomycete communities showed minimal, non-significant separation (**fig. S6b**). Taken together, the
246 *mmf1* mutant assembled a distinct bacterial root microbiome relative to wild-type plants, but only on
247 the BX_{plus} source microbiome.

a

Bacteria

	R^2	P
Line	**5.7**	**0.009**
BX_{minus}	4.6	0.605
BX_{plus}	**15.7**	**0.001**
Microbiome	3.9	0.088
Line:microbiome	**4.2**	**0.048**

Fungi

	R^2	P
Line	3.3	0.45
Microbiome	3.7	0.25
Line:microbiome	3.1	0.64

Oomycetes

	R^2	P
Line	3.3	0.23
Microbiome	5.5	**0.01**
Line:microbiome	3.2	0.24

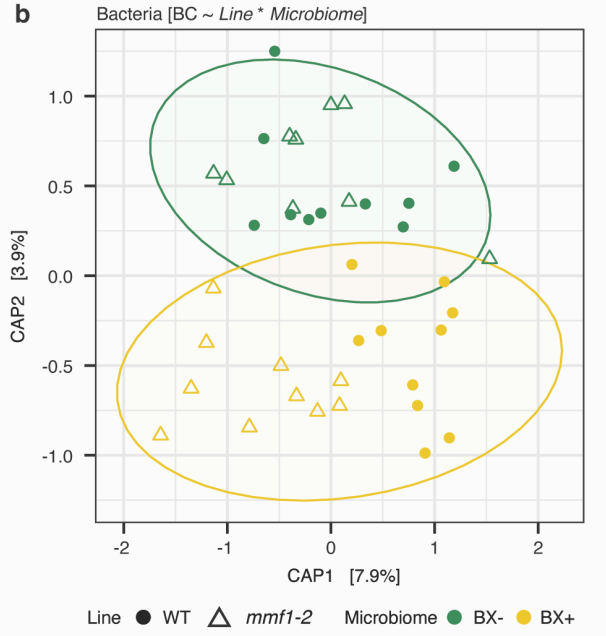

Figure 4. **Root microbiome profiling of wild-type and *mmf1-2* mutants grown on the BX_{plus} or BX_{minus} soil.** (**a**) The output of PERMANOVA on Bray-Curtis (BC) dissimilarities of bacterial, fungal and oomycete root microbiome of Arabidopsis wild-type (WT; Col-0) and *mmf1-2* mutants grown on the BX_{minus} or BX_{plus} soils (sampled from experiment IV, **Table S1**). The R^2 and p-values indicate the *line* and *microbiome* (conditioning) effects and their interaction. Pairwise PERMANOVA for bacterial communities compares WT and *mmf1-2* mutants on each soil condition; significant effects ($p < 0.05$) are indicated in bold. (**b**) Constrained Analysis of Principal Coordinates (CAP) for WT (filled circles) and *mmf1-2* mutants (open triangles) grown on the BX_{minus} (green) or BX_{plus} (yellow) soils confirming the effects of the soil conditioning and lines observed in the PERMANOVA analysis. Ellipses represent 95% confidence intervals for plants grown on BX_{minus} (green) or BX_{plus} (yellow) soils. Axes show the percentage of variance explained by the first two principal coordinates.

MMF1 is required for a defence-related transcriptional response

To obtain first insights into how MMF1 contributes to positive growth feedbacks, we analysed the root transcriptomes of wild-type and *mmf1-2* mutants in response to both soil microbiomes (detailed transcriptome analysis documented in **Dataset 6** and **Suppl. File 6**). Analogous to the microbiome analysis, we first examined the contributions of the factors *microbiome* (conditioning) and *line* on the transcriptome using PERMANOVA. *Microbiome* accounted for 29.0% (based on R^2, $p < 0.01$), *lines* for 33.7% ($p < 0.01$) and their interaction for 12.4% ($p < 0.01$) of the transcriptomic variation (**Fig. 5a**). Again, the significant interaction term revealed that mutant and wild type responded differently to the two soil microbiomes. Reduced pairwise PERMANOVA revealed again greater variation in wild-type (R^2 = 79.7%, $p < 0.01$) compared to mutant (R^2 = 10.8%, p = 0.349) plants in response to the two microbiomes. Principal Component (PC) analysis confirmed a clear separation between the two source microbiomes (PC1, 48% of variation) and plant lines (PC2, 16% of variance; **Fig. 5b**). Overall, the strongest separation was between wild-type plants in response to the two microbiomes, whereas the *mmf1* mutant transcriptomes clustered together.

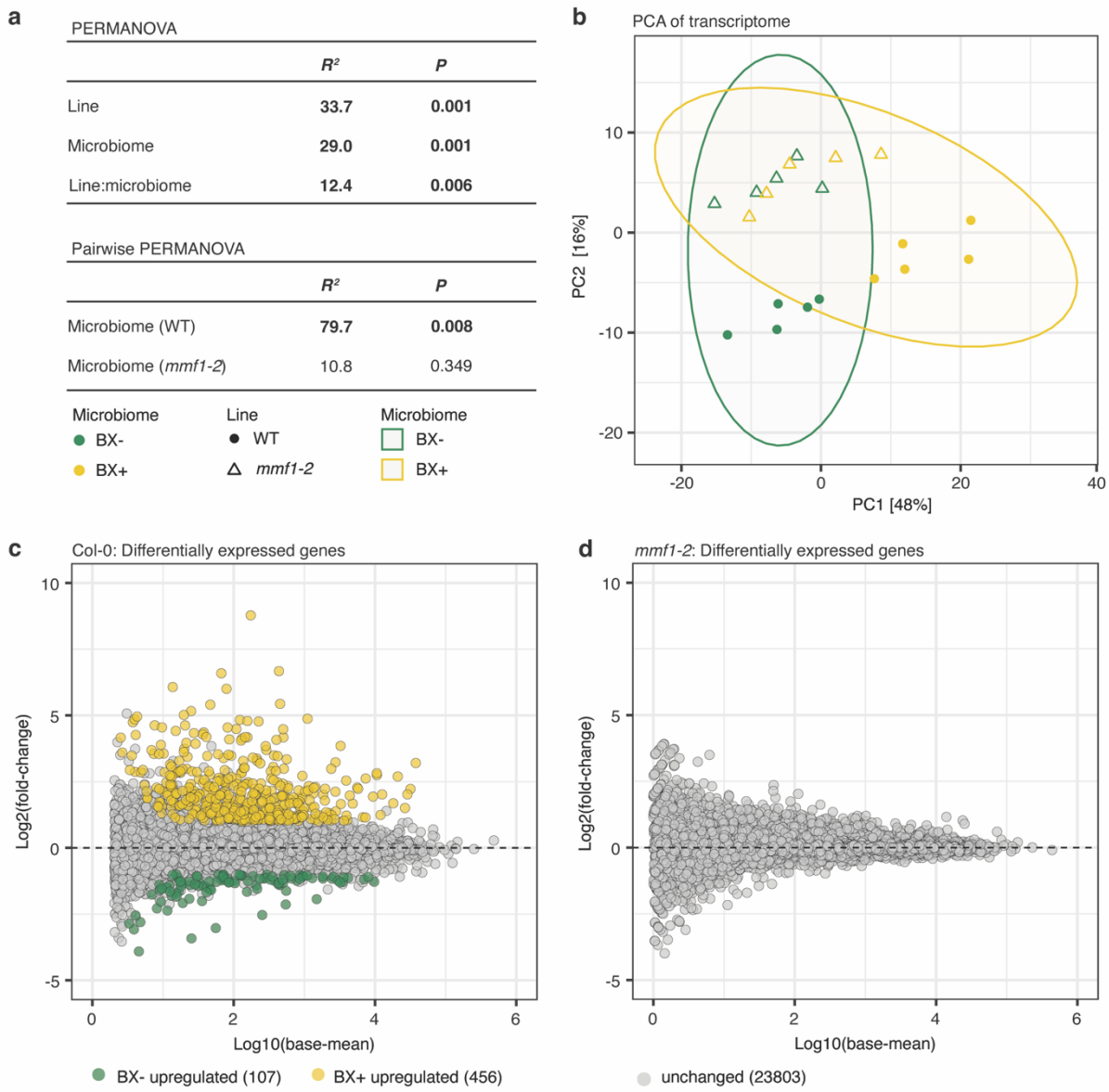

Figure 5. **Plants lacking MMF1 fail to mount a transcriptional response to a BX microbiome**. (**a**) The output of PERMANOVA on Bray-Curtis dissimilarities of the root transcriptome of wild-type (WT) and *mmf1-2* mutant plants in response to the BX_{minus} and BX_{plus} microbiomes (sampled from experiment IV, **Table S1**). The R^2 and *p*-values summarize the effects of *line* (plant genotype) and *microbiome* (soil condition) along with their interaction. Pairwise PERMANOVA results compare the transcriptomes of WT and *mmf1-2* mutant plants when grown on the BX_{minus} soil microbiome compared to the BX_{plus} soil microbiome; significant effects are indicated in bold. (**b**) Principal component analysis (PCA) of the same root transcriptome confirms the *line* (WT, closed circles; *mmf1-2*, open triangles) and *microbiome* (BX_{minus}, green; BX_{plus}, yellow) effect of the PERMANOVA results. The axes display the percentage of variance explained by each principal component. (**c**) MA plots illustrating differentially expressed genes (DEGs) in WT between BX_{minus} and BX_{plus} (left), and the absence of DEGs in *mmf1-2* (right). Genes upregulated on the BX_{plus} microbiome (yellow) or BX_{minus} microbiome (green) are colour coded. Genes with a $\log_2$ fold-change ≥ 1 and false discovery rate < 0.05 (empirical Bayes' shrinkage; DESeq2) are considered significant.

Next, we analysed the transcriptomes at gene level determining differentially expressed genes (DEGs; $\log_2$ fold-change ≥ 1; empirical Bayes shrinkage, *p* values adjusted for false discovery rate < 0.05).

292 Aligned with the microbiome analysis (**Fig. 4**), we found more DEGs between the lines in response to
293 the BX_{plus} (347 total; 230 up and 117 down in wildtype) compared to the BX_{minus} soil microbiome (128
294 total; 68 up and 60 down; **fig. S7**). Wild-type plants had 563 DEGs in response to the two microbiomes
295 (107 down and 456 up, **Fig. 5c**). Surprisingly, not a single microbiome specific DEG was found in
296 mutant plants (**Fig. 5d**). Taken together, a functional MMF1 leads to a strong transcriptional
297 reprogramming, mostly in response to the BX_{plus} soil microbiome.
298 Finally, we performed co-expression and gene ontology (GO)-term enrichment analysis
299 (underlying genes documented in **Dataset 6**) to characterise the transcriptional changes of wild-type
300 plants in response to the two microbiomes (**Fig. 5c**). Hierarchical clustering identified clusters of co-
301 expressed genes: four up- and three downregulated (**fig. S8**). Upregulated processes included hypoxia
302 (clusters #2 and #3) and immune responses (clusters #2 to #5). Processes linked to hypoxia included
303 the GO terms response to hypoxia and cellular response to hypoxia (**Dataset 6**). Upregulated immune
304 processes included GO terms such as response to ethylene and systemic acquired resistance (cluster
305 #2), defence response to insects, and response to bacterial molecules (cluster #3), indole metabolism
306 and response to salicylic acid (SA; cluster #4), and hypersensitive response, programmed cell death,
307 and interaction with symbionts (cluster #5; see **Dataset 6** for the genes in each cluster). Of note, several
308 of these genes are typically involved in TNL-triggered immunity (*39*, *42*). Downregulated processes
309 included fatty acid biosynthesis, secondary metabolite biosynthesis and malate transport (clusters #6 to
310 #8; **Dataset 6**). In conclusion, wild-type plants, which achieved better growth in response to the BX_{plus}
311 soil microbiome, exhibited a strong transcriptional reprogramming, most noticeably an upregulation of
312 defence-related genes.
313

314 **Discussion**

315 While genotype-dependent microbiome feedbacks have been observed in many plant systems (*14*, *28*,
316 *29*, *32*), the mechanisms underlying plant responses to complex microbiomes remain largely
317 unresolved. Here, we used natural variation in growth feedbacks to BX_{plus} and BX_{minus} soil microbiomes
318 among Arabidopsis accessions (**Fig. 1c**) to uncover candidate loci through which plants respond to
319 different microbiomes in natural soils. We focussed on the gene AT3G44630, which was in the
320 proximity of the top SNP in GWAS (**Fig. 2**), named this TNL receptor gene *MMF1* and characterized
321 it in the reference accession Col-0. Arabidopsis *mmf1* mutants lack three hallmarks of wild-type plants
322 in response to the BX_{plus} soil microbiome: they lose the positive growth feedback (**Fig. 3**), have an
323 altered root bacterial community (**Fig. 4**), and fail to trigger the defence-related transcriptional response
324 (**Fig. 5**). Given the molecular function of TNLs - to recognise microbial effectors intracellularly and
325 trigger ETI (*20*) – our results support the following mechanistic model (**fig. S9**): When grown on the
326 BX_{plus} soil microbiome, wild-type plants show enhanced shoot growth resulting from a defence-related
327 transcriptional response (**fig. S8**). This MMF1-dependent transcriptional response, together with the
328 typical intracellular localisation of TNLs, imply that a bacterial (see below) effector of the BX_{plus}
329 microbiome is perceived inside the root cells. This model is consistent with the reduced shoot growth
330 of wild-type plants on the BX_{minus} microbiome (in the absence of the effector) as well as *mmf1* mutants
331 on the BX_{plus} microbiome (lack of the receptor), and is further supported by the lack of a defence-related
332 transcriptome in *mmf1* mutants.

333 The plant responses, including a defence-related transcriptome and enhanced shoot growth,
334 coincided with an altered root microbiome (**fig. S8**). While overall root microbiomes were similar
335 between soil sources, the bacterial communities of wild-type and *mmf1* mutant plants differed
336 significantly on the BX_{plus} but not on the BX_{minus} microbiome (**Fig. 4**). These data do not allow to
337 establish a causal link between the altered root microbiome and the differential shoot growth of the
338 genotypes. However, the observation suggests that a bacterial effector in the BX_{plus} microbiome, which
339 presumably triggers the defence-related transcriptome via the TNL MMF1, may be responsible.
340 Identification of the bacterial species and the actual effector are obvious future research targets.

341 As part of the immune system, TNLs act as gatekeepers against opportunistic pathogens,
342 maintaining host health and microbiome homeostasis (*20*). Earlier work showed that Arabidopsis with
343 impaired ETI undergo microbiome dysbiosis in their leaves, and ultimately these plants have reduced
344 fitness (*24*, *43*). Analogously, in roots, we report microbiome dysbiosis in the ETI mutant *mmf1* and
345 demonstrate that MMF1 is required for growth promotion in wild-type plants. Both examples imply
346 that TNLs integrate microbiome signals inside host cells for maintaining microbiome homeostasis and
347 host health. While TNLs have been predominantly studied in single-pathogen and gene-for-gene
348 interactions, they face a multiplicate challenge at the microbiome level, with many more effectors being
349 present in a diverse microbiome (*16*). Thus, plant immune responses rely on more complex signal
350 integration when interacting with microbial communities compared to single isolates (*16*, *43*).

351 Moreover, there is evidence that signal integration may further depend on TNL receptor dosage:
352 recently, high TNL copy numbers within the *RPP-1*-like gene cluster among Arabidopsis accessions
353 were linked with reduced bacterial diversity in their phyllosphere (*44*). Of note, the closest homolog of
354 MMF1 is Recognition of Peronospora Parasitica 1 (RPP1) (*45*), and additional TNLs are in the
355 proximity of the SNP most strongly associated with the variation in growth feedback among the tested
356 accessions (**Fig. 2b**). Here, we have shown that lack of MMF1 is sufficient for the loss of growth
357 feedback, but future work is needed to test whether additional members of the TNL family or their
358 dosage also contribute to feedback in other accessions.
359 We set out to identify a first genetic component through which plants respond to different
360 microbiomes in natural soils. The substantial variation in growth feedbacks among Arabidopsis
361 accessions (**Fig. 1c**) implies that there are additional components to discover. The TNL MMF1 presents
362 a first genetic component for such feedbacks, but for now it only explains the enhanced growth and
363 increased defence of the reference accession Col-0 responding to the BX_{plus} microbiome. MMF1 and
364 the top SNP in its proximity alone cannot explain the massive variation in growth feedbacks among the
365 other accessions. For instance, Hadd-3, which shares the reference allele of the top SNP with Col-0,
366 grew more poorly on the BX_{plus} microbiome, while IP-Hue-3 harboured the alternative allele and grew
367 much better than Col-0. Solving this puzzle requires further analysis of the complex locus around the
368 top SNP (*44*), and investigating the MMF1 alleles of the extreme accessions such as Hadd-3 and IP-
369 Hue-3. Together with the other GWAS candidate loci (**Fig. 2a**), additional genetic components likely
370 contribute to explaining the massive variation in growth feedbacks among the accessions.
371 In conclusion, the identified TNL receptor provides a relatively straightforward explanation for
372 the enhanced shoot growth of Col-0 on the BX_{plus} soil microbiome: MMF1 perceives an effector of the
373 BX_{plus} microbiome, triggers defences, and alters the root microbiome, which collectively coincide with
374 better shoot growth by yet unknown mechanisms. This work contributes to understanding host genetic
375 pathways by which plants perceive complex soil microbiomes and mediate microbiome feedbacks.
376 Such knowledge may pave the way towards crops that leverage beneficial microbiome feedbacks,
377 ultimately improving yield in a more sustainable manner.
378
379

Materials and methods

Plant material

The maize (*Zea mays* L.) genotypes B73 and *bx1* (B73) transposon insertion mutant (*46*) were used for soil conditioning (see below). The 410 *Arabidopsis thaliana* (hereafter: Arabidopsis) accessions used in the GWAS (see below) were obtained from the 1001 genomes project (The 1001 Genomes Consortium, 2016). For a full list of the accessions used, see **Dataset 1**. Arabidopsis T-DNA insertion mutants (AT3G44630) for *mmf1-1* (SALK_144159C) and *mmf1-2* (SALK_002318C) are in the Col-0 background and were obtained from the Nottingham Arabidopsis Stock Centre (NASC). Mutants were confirmed for homozygosity and characterised by qPCR (**fig. S4;** primers in **Table S3**). The mutant lines *eds1-12* (*40*), *pad4-1* (*47*), and *sag101-3* (*48*) in Col-0 background were kindly provided by Prof. Jane Parker.

Generation of BX_{minus} and BX_{plus} soil microbiomes

We used soil from an agricultural field site of Agroscope in Changins, Switzerland (46°24'00.0"N6°14'22.8"E; three adjacent plots, Parcel 29, Parcel 30, or Parcel 31) and we generate the distinct soil microbiomes either in the field or in the greenhouse using pots filled with that soil. Starting from replicates of the same batch of unconditioned field soil, the two distinct microbiomes are generated by growing of either wild-type maize (B73), which secrete benzoxazinoids (BXs) to the surrounding soil, or BX-deficient mutant maize (*bx1* (B73)). After three months of growth, the plants and roots are removed and the two maize lines "leave behind" BX-conditioned (BX_{plus}) and control (BX_{minus}) microbiomes in the soil. We then harvest either replicate soil cores (20 × 20 × 20 cm, conditioning in the field) or soil from replicate pots (3 L, 13.1 cm deep and 20.2 cm diameter; conditioning in the greenhouse), sieve the soil through a 1 cm^2 sieve and stored it at 4°C until the subsequent feedback experiments. We described in detail the approach of generating BX_{minus} and BX_{plus} soil microbiomes (we often referred to this as 'soil conditioning') including the physicochemical characteristics of the soil (*14*, *28*, *37*), management practices and cropping history of the field site (*14*, *26*) and the conditions for greenhouse conditioning (*14*, *28*, *30*). The batches of conditioned soils for this study, and the experiments linked to soil batches are listed in **Table S1** and **S2**.

Microbiome feedback experiments

We list the setups and purposes of different experiments (Exp. I to Exp. VI) with Arabidopsis grown on BX_{minus} and BX_{plus} soil microbiomes in **Table S2**. For feedback experiments, the replicate soil samples containing the BX_{plus} and BX_{minus} microbiomes were individually amended with sand, by manually mixing in 20% (v/v) autoclaved quartz sand (*14*). Pots were equally filled by weight and randomized across trays. Below we detail the specific setups and conditions for the high-throughput phenotyping of the different Arabidopsis accessions (Exp. I and II) and the characterisation of wild-type and mutant lines in Col-0 background (Exp. III - VI).

417 *High-throughput phenotyping of Arabidopsis accessions:* We performed two microbiome
418 feedback experiments; each experiment was done with 210 accessions (10 accessions repeated in both
419 runs) resulting in a total of 410 tested Arabidopsis genotypes (**Dataset 1**). In each experiment, every
420 accession was seeded on both BX_{minus} and BX_{plus} soils with 3 replicates (2 experiments of 210 accessions
421 x 2 soils x 3 replicates = 1260 pots). Plant cultivation and phenotyping was previously described and
422 the images of the first experiment were utilized to develop the phenotyping software ARADEEPOPSIS
423 (without comparing BX_{minus} and BX_{plus} soils) (*34*). In brief, plants were grown at the Gregor Mendel
424 Institute of Molecular Plant Biology, Vienna, Austria, in a custom-built growth chamber (YORK
425 Refrigeration), equipped with an environmental control unit (Johnson Controls) and a climate control
426 unit (Incotec) under long-day conditions (16h light [21°C], 8h dark [16°C], 140 $\mu E/m^2s$) with 60 %
427 relative humidity and watered twice per week by flooding. Plants were imaged twice daily, and plant
428 morphometric phenotypes extracted using the phenotyping software ARADEEPOPSIS (*34*). The
429 phenotypes were converted into "days after germination" phenotypes by taking the average of the two
430 measurements that happened on the same day. **Dataset 1** contains the source data and **Suppl. File 1**
431 documents the analysis.
432 *Feedback experiments with Arabidopsis mutants:* For microbiome feedback experiments
433 performed on Arabidopsis Col-0 mutant lines, we used greenhouse conditioned soils prepared as
434 described before. Seeds were stratified for 3 days in the dark at 4 °C and sowed on pots (5.5 × 5.5 × 5
435 cm) filled by weight. Plants were grown in a plant growth chamber (Percival, CLF Plant Climatics,
436 Wertingen, Germany) under short days with 10h light (100 $\mu mol\ m^{-2}\ s^{-1}$) (21 °C) and 14h darkness (18
437 °C) at 60% relative humidity. Plants were fertilized at day 14 and 21 after germination using 10 mL of
438 1:3 times diluted ½ strength Hoagland solution (*49*), watered 3 times per week by weight, and
439 randomized weekly. Analysis was blinded by adding barcodes to the pots for phenotyping which was
440 used to trace back sample names after analysis. Plants were photographed weekly and phenotyped using
441 the ARADEEPOPSIS pipeline to obtain the rosette area (plant region area) (*34*). Plants were grown for
442 6 weeks before the rosettes and roots were harvested for downstream analysis. **Dataset 4** contains the
443 source data and **Suppl. File 4** documents the analysis.
444
445 ***Genome-wide association study***
446 Genome-wide association studies (GWAS) search for associations between single nucleotide
447 polymorphisms (SNPs) in a genome and a phenotype (*50*). As phenotype we took the differential growth
448 feedback of the accessions on the two soil microbiomes, i.e. the mean growth on BX_{minus} was subtracted
449 from the mean growth on BX_{plus} soil microbiomes [$BX_{plus} - BX_{minus}$]. We focussed on the first 20 days
450 after germination (DAG) to avoid confounding effects of phenotypes like early flowering and
451 overlapping leaves. GWA was performed using an in-house Nextflow pipeline
452 (https://gitlab.lrz.de/beckerlab/gwas-nf) that wraps limix (*38*) and applies the same multi-trait model
453 used previously in Huether et al. 2020. Only SNPs with a minor allele frequency of at least 1% were

454 included. The model estimates each SNP's "specific" effect on the trait "differential growth feedback".
455 In this study, we used plant_region_area as a trait (**Dataset 1**), and the specific effect reflects the
456 difference in that measurement between the soil conditions. The analysis was conducted independently
457 for each day because we noted temporal variation in daily growth feedbacks, and the resulting tables
458 were combined without re-adjusting the corrected p-values. SNPs were retained and visualized if they
459 had a $-\log_{10}$(adjusted p-value) of at least 5 on at least three consecutive days and a minor allele count
460 of at least 5. From these plots, we identified SNPs with a robust multi-day signal and analysed them
461 further using gwaR (https://github.com/Gregor-Mendel-Institute/gwaR). This allowed us to investigate
462 the genomic neighbourhood of those SNPs and pinpoint genes likely involved in the microbiome
463 feedback phenotype. Detailed approach to select candidate genes is explained in **Suppl. Text**. The
464 GWAS data are in **Dataset 3** and their analysis is documented in the **Suppl. File 3**. For computational
465 analyses, we used the BioHPC-Genomics compute cluster at the Leibniz Rechenzentrum and the CLIP
466 cluster at Vienna BioCenter (VBC).
467
468 ***GWAS candidate gene selection***
469 To identify candidate genes associated with BX-growth feedbacks, we performed the genome wide
470 association study (GWAS) with the 410 genome-sequenced accessions using their phenotypic diversity
471 in growth feedbacks (**Fig. 1c**). To account for population structure within the *Arabidopsis* accessions,
472 a linear mixed model was employed (*38*). We used the daily growth feedback data, which includes the
473 temporal dynamics (**fig. S2a**), and calculated associations between single nucleotide polymorphisms
474 (SNPs) and phenotypes for each of the 20 DAGs (**Dataset 3**). In essence, we performed the GWAS
475 using each day as a covariable in the analysis.
476 To impose stringency in SNP identification, we performed FDR correction and Bonferroni
477 correction of the *p*-values of SNPs that associated with the growth feedbacks (**Fig. 2a**, **Dataset 3**). Next,
478 we filtered the SNPs for those with a minor allele frequency of higher than 2.5 % to also include rare
479 SNPs associated with local and environmental adaptation (*51*), and those SNPs with significance
480 (Bonferroni correction) for at least three consecutive days. To isolate candidate genes, we used the
481 "get_nearest_genes" function from the gwaR package in R (https://github.com/Gregor-Mendel-
482 Institute/gwaR) to identify genes located near each candidate SNP. Finally, to select candidate genes
483 for functional validation, we screened the genes identified in the GWAS for overlap with differentially
484 expressed genes in the roots and shoots of Arabidopsis plants grown on a BX_{minus} and BX_{plus} microbiome
485 (*30*).
486
487 ***MBOA allelopathic growth assays***
488 To test for the allelopathic effect of MBOA on plant growth, we grew different Arabidopsis accessions
489 on ½ MS (Duchefa, Haarlem, the Netherlands) plates containing 1.5% phytoagar (Duchefa, Haarlem,
490 the Netherlands) supplemented with 0.25 mM MBOA (Sigma Aldrich, St. Louis, USA) dissolved in

491 DMSO or on control plates supplemented with the same concentration (500 µL per L) of DMSO (*52*).
492 Seeds were stratified by incubating plates for 3 days at 4 °C. The plates were placed upright and grown
493 in a controlled growth chamber (Percival, CLF Plant Climatics, Wertingen, Germany) in short days
494 with 10 hours light (100 µmol m^{-2} s^{-1}) (21 °C) and 14 hours darkness (18 °C) at 60 % relative humidity.
495 After 10 days, the lateral root length was measured using the image software ImageJ (*53*).
496
497 ***Root microbiome profiling***
498 *DNA extraction:* For root microbiome analysis, 10 randomly selected *Arabidopsis* root systems were
499 removed from the pots, and excess soil carefully removed by hand. The root system was rinsed with
500 sterile ddH_2O to remove additional soil. The entire root system was flash frozen in liquid nitrogen and
501 stored at -80 °C until further processing. The roots were lyophilized for 24 h and grinded in 1.5 mL
502 Eppendorf tubes using a Retsch mill (Retsch GmBH, Haan; Germany) and 2 mm glass beads at 30 Hz
503 for 1 min. Approximately 20 mg of dry root material was used as the input for DNA extractions. DNA
504 extractions were performed in 96-well plates using the QIAGEN® MagAttract® PowerSoil® DNA KF
505 Kit (Qiagen, Germany) and the KingFisher™ Flex™ Purification System (ThermoFisher Scientific,
506 Waltham, MA) following the manufacturers guidelines. For all samples, the DNA concentration was
507 determined using the AccuClear® Ultra High Sensitivity dsDNA Quantitation Kit (Biotum, Fremont,
508 United States). For library preparation, DNA concentration was adjusted to 2 ng/µL with a Myra Liquid
509 Handler (Bio Molecular Systems, Upper Coomera; Australia), and 10 ng used for library preparation.
510 *Library preparation:* Library preparation for bacteria, fungi and oomycetes was performed
511 using an adapted two-step barcoded host-associated microbiome hamPCR protocol (*54*). Primers used
512 are documented in **Table S3**. For bacteria, the first PCR was performed using a combination of the
513 CS1-*fs*-799-F and CS2-*fs*-1193R frameshift (fs) (pooled in 5 equimolar concentrations) in
514 combination with the host specific *GIGANTEA* CS1-At-GI-F and CS2-At-GI-R primers in a single well.
515 We followed earlier work PCR settings for annealing temperature (*55*) and cycling conditions (*54*).
516 Briefly, the PCR settings were 94 °C for 2 min, and 10 cycles of 94 °C for 30 s, 55 °C for 50 s, 72 °C
517 for 30 s and finally 72 °C for 5 min. For fungi, the first PCR was performed with the internal transcribed
518 spacer (ITS) region primers ITS1fF and ITS2R with standard temperature (*56*) and cycle (*54*) settings.
519 The PCR settings were 94 °C for 3 min, and 10 cycles of 94 °C for 45 s, 50 °C for 60 s, 72 °C for 90 s,
520 and finally 72 °C for 10 min. For oomycetes, we adapted the ITS1-O_F1_G-46636 and 5.8s-O_R1_G-
521 46637 primers (*54*) with the CS1 and CS2 adapter sequences and utilised the same PCR settings as for
522 the fungi. PCR amplicons were purified using the ChargeSwitch® PCR Clean-Up Kit (Invitrogen,
523 Waltham, MA, USA) on a KingFisher™ Flex™ Purification System (ThermoFisher Scientific,
524 Waltham, MA, USA). The second PCR added unique barcodes to 5 µL of purified DNA using the
525 Fluidigm Access Array barcoding primers (Standard BioTools, California, USA). The cycling
526 conditions were 94 °C for 2 min, 25 cycles of 94 °C for 30 s, 60 °C for 30 s, 72°C for 60 s, and finally
527 extension 72°C for 10 min. Samples were again purified as before and quantified and pooled by adding

528 80 ng of each sample using a Myra Liquid Handler to create sub-libraries for bacteria, fungi and
529 oomycetes. The pooled bacterial sub-library was subsequently separated on an 1.5 % agarose gel, the
530 bacterial and GIGANTEA fragments excised, and gel purified using the Wizard® SV Gel and PCR
531 Clean-Up System (Promega, Madison, Wisconsin, USA). The final bacterial sub-library was created by
532 scaling the purified bacterial and GIGANTEA amplicons in a 24:1 ratio (bacteria:GIGANTEA) to
533 reduce the amount of plant reads during sequencing. Five random samples were duplicated during
534 library preparation and left unscaled to bioinformatically rescale the scaled samples (see ref (*54*) for
535 details). The final sequencing library was created by pooling the sub-libraries in a DNA ratio of 87.5%
536 (963 ng) scaled bacteria, 5.5 % (60 ng) unscaled bacterial samples and 3.5 % (39 ng) each for fungal
537 and oomycetes. The library was paired end sequenced on an Illumina MiSeq instrument (v3 chemistry,
538 300 bp paired end) at the NGS platform (https://www.ngs.unibe.ch) of the University of Bern.
539 *Bioinformatics*: MiSeq reads were quality checked with FastQC v0.11.8 (Babraham Institute,
540 Cambridge, United Kingdom). Barcodes were removed previously by the NGS platform and written to
541 the sequence headers. With this information the data was demultiplexed and primers were removed
542 using cutadapt v3.4 (*57*). Following the methods from (*29*), quality filtering, read merging and amplicon
543 sequence variant (ASV) infering was performed with the dada2 package v1.26.0 (*58*) in R v4.2.0 (R
544 Core Team 2022). Taxanomic assignment were done using naïve Bayesian classifier with a DADA2
545 formatted version from the SILVA v. 132 database (*59*) for bacteria and the FASTA general release
546 from UNITE v8.3 for fungi. To improve taxonomy assignment, the taxonomy was assigned again with
547 the IDTAXA classifier using the SILVA r138 and UNITE 8.2 databases from DECIPHER v2.26.0 (*60*)
548 and replaced wherever IDTAXA assigned more taxonomic levels than the naïve Bayesian classifier.
549 Bacterial ASVs assigned as Eukarya, Archaea, Cyanobacteria or Mitochondria and fungal ASVs
550 belonging to Protista, Plantae, Protozoa or Animalia were discarded. Calculations were performed at
551 the sciCORE (http://scicore.unibas.ch/) scientific computing center of the University of Basel.
552 *Statistical analysis:* Statistical analyses were performed with the vegan package v.2.6.4 (*61*) in
553 R v4.2.0. Following the strategies described before (*62*), we normalised the data for bacteria, fungi and
554 oomycetes by rarefication. Rarefaction thresholds per sample were defined as 6.02×10^4 for bacteria,
555 800 for fungi and 5700 for oomyctes (*62*). Outlier detection was performed with CLOUD using Bray-
556 Curtis (BC) distances from the rarefied data for each condition and each treatment individually (*63*).
557 The nearest number of neighbours were set to 60% of the sample size and we chose an empirical outlier
558 percentile of 0.1. As described before (*54*), microbe-to-host ratios were reconstructed and the microbial
559 load of each sample was quantified. Using a count table scaled by the microbial load, we performed
560 ordinations based on Bray-Curtis dissimilarity matrices using R package phyloseq (*64*) and visualised
561 it in a Constrained analysis of principle coordinates (CAP). We performed Permutational Multivariate
562 Analysis of Variance (PERMANOVA) with 999 permutations with the adonis function from the vegan
563 package to quantify the effects of our experiment. The microbiome data is in **Dataset 5** and its analysis
564 is documented in **Suppl. File 5**.

565 ***Transcriptome analysis***

566 *RNA extraction, library preparation and sequencing:* Roots from 6-week-old Arabidopsis plants were
567 carefully removed from the soil. Excess soil was removed by briefly rinsing the roots in sterile ddH_2O
568 and dried using a paper towel. The roots were then flash frozen in liquid nitrogen and homogenized in
569 a 1.5 mL Eppendorf tube using a plastic micro pestle (Carl Roth, Karlsruhe, Germany). Total RNA was
570 extracted using the RNeasy Plant Mini Kit (Qiagen, Hilden, Germany) with on-column DNase
571 treatment with the RNase-Free DNase kit (Qiagen, Hilden, Germany) following the manufacturer's
572 protocol. RNA integrity was assessed using a Fragment Analyzer (Agilent Technology, Santa Clara,
573 California, USA). RNA concentration was determined fluorometrically using the Qubit RNA HS Assay
574 Kit (Thermo Fisher, Waltham, Massachusetts, USA). Libraries were prepared using the TruSeq
575 Stranded mRNA kit (Illumina, SanDiego, California, USA) with 200 ng total RNA as input. Library
576 preparation and sequencing was performed at the Genomics Facility
577 (https://bsse.ethz.ch/genomicsbasel) of the University of Basel. Sequencing (51 bp paired end) was
578 performed on an Illumina Novaseq® 6000 System (Illumina, SanDiego, California, USA) with an SP
579 slow cell.

580 *Bioinformatics and statistics:* Reads were aligned to the *Arabidopsis thaliana* TAIR10
581 reference genome and read counts determined using STAR 2.7.9a (*65*). The raw data processing was
582 performed at the scientific computing facility of the University of Basel (http://scicore.unibas.ch/).
583 Sample outliers were identified using a combination of generalized principal component analysis and
584 by analysing Poisson distances across samples. Sample clustering was performed using variance
585 stabilizing transformations on the normalized gene counts. Differential gene expression analysis was
586 performed in R using DESeq2 (*66*), a method for differential analysis of count data using a **negative**
587 **binomial** generalized linear model **with shrinkage estimation of dispersions** and fold changes. Co-
588 expression analysis was performed with the R package coseq v1.18.0 (*67*). Clustering of the co-
589 expressed genes was performed by running a Gaussian mixture model and arcsine transformation of
590 normalized expression profiles 20 times to identify the optimal number of clusters (*67*). The
591 transcriptomic data is in **Dataset 6** and the documented analysis in **Suppl. File 6**.

592

593 ***Validation of single T-DNA insertion in mmf1-2***

594 We validated that *mmf1-2* carries a single T-DNA insertion by long-read whole genome sequencing and
595 reference-guided assembly. High molecular weight DNA was extracted from leaves using the Machery-
596 Nagel NucleoBond HMW DNA kit according to manufacturer's instructions. Long-read sequencing
597 was carried out on an Oxford Nanopore Technologies promethion 24 instrument in a multiplexed run
598 on a R10.4 flow cell. After demultiplexing with dorado (https://github.com/nanoporetech/dorado)
599 adapters were trimmed using porechop, and the genome was assembled using flye (*68*), polished with
600 medaka (https://github.com/nanoporetech/medaka) and scaffolded against Col-CEN (*69*) using ragtag
601 (*70*) and annotations (araport11) from Col-CEN were lifted over using liftoff (*71*). The T-DNA insertion

602 in AT3G44630 was identified by aligning to the reference genome. The T-DNA sequence was used as
603 a query for BLAST against the *mmf1-2* assembly, returning only the insertion in AT3G44630 (**fig. S4d**).
604
605 ***Statistical analysis***
606 We used R (R core Team, 2016) for statistical analysis and visualization of data. The R version and
607 package version used for each step of the analysis is documented at the end of the markdown files. All
608 the code required to reproduce the statistical analysis and graphing can be found on the GitHub
609 repository of this article. Figures were exported from R and combined and formatted using Adobe
610 Illustrator. The appropriate statistical test used for each analysis is indicated in the corresponding
611 figure legends and is annotated in the available code.
612
613 **Data availability**
614 We have deposited all source data together with all analysis scripts underlying all figures on GitHub
615 (https://github.com/PMI-Basel/JansevanRensburg_et_al_GWAS_MMF1). The GitHub repository's
616 structure follows the structure of this manuscript with separate folders of source data and analysis scripts
617 on i) Accession growth feedback (Dataset 1), ii) MBOA sensitivity (Dataset 2), iii) GWAS statistics
618 (Dataset 3), iv) Col-0 and mutant growth feedback (Dataset 4), v) microbiome (Dataset 5) and vi)
619 transcriptome (Dataset 6). Each dataset and its analysis documentation (R-markdown outputs) is shared
620 with this article as **Dataset 1** to **6** and the corresponding **Suppl. Files 1** to **6**. The raw sequencing data
621 are stored at the European Nucleotide Archive (http://www.ebi.ac.uk/ena). The microbiome profiling is
622 stored under project number PRJEB85607, the transcriptome data is available under PRJEB85599 and
623 the genome of the *mmf1-2* mutant under PRJEB85789. The bioinformatic code of all analyses, including
624 information on barcodes, primers and sample assignments is provided on GitHub. Raw images are
625 available upon request.
626
627

Code availability

All the code required to reproduce the statistical analysis and graphing can be found on GitHub https://github.com/PMI-Basel/JansevanRensburg_et_al_GWAS_MMF1.

Acknowledgements

We specifically thank Nicolas Widmer from Agroscope Changins (Switzerland) for field access and assistance. We thank Prof. Jane Parker for providing Arabidopsis mutant seeds. We thank the team at the Plant Sciences Facility at Vienna BioCenter Core Facilities GmbH (VBCF), a member of the Vienna BioCenter (VBC), Austria, for their help with Arabidopsis image acquisition. We are very grateful to Dr. Pamela Nicholson and her team at the Next Generation Sequencing Platform in Bern for excellent technical support. We thank Dr. Phillipe Demougin and Dr. Christian Beisle (both University of Basel, Switzerland) for their support with RNAseq. Finally, we thank Duncan Crosbie (LMU Munich) and Helmut Blum and Stefan Krebs (Gene Center, LMU Munich) for support with genome sequencing of *mmf1-2*.

Funding

This project was funded by the Swiss National Foundation (Grant No. 189249 to K.S.), the Austrian Academy of Sciences (ÖAW, to C.B.), by the European Union's Horizon 2020 research and innovation programme by the European Research Council (ERC) (Grant Agreement No. 716823 'FEAR-SAP' to C.B.). N.S. received funding from the Deutsche Forschungsgemeinschaft (DFG) in the frame of TRR356 project A05 (project No. 491090170). For parts of the computational analyses, we used the BioHPC-Genomics compute cluster at the Leibniz Rechenzentrum Munich (DFG; grant no. 450674345) and the CLIP batch environment at the Vienna Biocenter.

Ethics declarations

None

References

1. P. Trivedi, J. E. Leach, S. G. Tringe, T. Sa, B. K. Singh, Plant–microbiome interactions: from community assembly to plant health. *Nature Reviews Microbiology* **18**, 607–621 (2020).

2. R. L. Berendsen, C. M. J. Pieterse, P. A. H. M. Bakker, The rhizosphere microbiome and plant health. *Trends in Plant Science* **17**, 478–486 (2012).

3. R. Mendes, P. Garbeva, J. M. Raaijmakers, The rhizosphere microbiome: Significance of plant beneficial, plant pathogenic, and human pathogenic microorganisms. *FEMS Microbiology Reviews* **37**, 634–663 (2013).

4. W.-J. Li, X.-Y. Zhou, X.-L. An, L.-J. Li, C.-S. Lin, H. Li, H.-Z. Li, Enhancement of beneficial microbiomes in plant–soil continuums through organic fertilization: Insights into the composition and multifunctionality. *Soil Ecol. Lett.* **6**, 230223 (2024).

5. H. Janse van Rensburg, K. Stengele, K. Schlaeppi, Understanding plant responsiveness to microbiome feedbacks. *Current Opinion in Plant Biology* **81**, 102603 (2024).

6. T. M. Bezemer, C. S. Lawson, K. Hedlund, A. R. Edwards, A. J. Brook, J. M. Igual, S. R. Mortimer, W. H. Van Der Putten, Plant species and functional group effects on abiotic and microbial soil properties and plant-soil feedback responses in two grasslands. *Journal of Ecology* **94**, 893–904 (2006).

7. W. H. Van der Putten, R. D. Bardgett, J. D. Bever, T. M. Bezemer, B. B. Casper, T. Fukami, P. Kardol, J. N. Klironomos, A. Kulmatiski, J. A. Schweitzer, K. N. Suding, T. F. J. Van de Voorde, D. A. Wardle, Plant-soil feedbacks: The past, the present and future challenges. *Journal of Ecology* **101**, 265–276 (2013).

8. M. A. Meier, G. Xu, M. G. Lopez-Guerrero, G. Li, C. Smith, B. Sigmon, J. R. Herr, J. R. Alfano, Y. Ge, J. C. Schnable, J. Yang, Association analyses of host genetics, root-colonizing microbes, and plant phenotypes under different nitrogen conditions in maize. *eLife* **11** (2022).

9. Y. Song, E. Atza, J. J. S. Gil, D. Akkermans, R. de Jonge, P. G. H. de Rooij, D. Kakembo, P. A. H. M. Bakker, C. M. J. Pieterse, N. V. Budko, R. L. Berendsen, Seed tuber microbiome is a predictor of next-season potato vigor. *bioRxiv*, 2024.04.18.590071 (2024).

10. M. Wang, A.-H. Ge, X. Ma, X. Wang, Q. Xie, L. Wang, X. Song, M. Jiang, W. Yang, J. D. Murray, Y. Wang, H. Liu, X. Cao, E. Wang, Dynamic root microbiome sustains soybean productivity under unbalanced fertilization. *Nat Commun* **15**, 1668 (2024).

11. R. C. Wilhelm, H. M. van Es, D. H. Buckley, Predicting measures of soil health using the microbiome and supervised machine learning. *Soil Biology and Biochemistry* **164**, 108472 (2022).

12. X. Qiao, S. Bei, G. Wang, C. Li, H. Li, J. Zhang, F. Zhang, Soil biota is decisive for overyielding in intercropping under low phosphorus conditions. *Journal of Applied Ecology* **59**, 1804–1814 (2022).

13. M. Chialva, A. Salvioli di Fossalunga, S. Daghino, S. Ghignone, P. Bagnaresi, M. Chiapello, M. Novero, D. Spadaro, S. Perotto, P. Bonfante, Native soils with their microbiotas elicit a state of alert in tomato plants. *New Phytologist* **220** (2018).

14. L. Hu, C. A. M. Robert, S. Cadot, X. Zhang, M. Ye, B. Li, D. Manzo, N. Chervet, T. Steinger, M. G. A. Van Der Heijden, K. Schlaeppi, M. Erb, Root exudate metabolites drive plant-soil feedbacks on growth and defense by shaping the rhizosphere microbiota. *Nature Communications* **9**, 1–13 (2018).

15. P. J. P. Teixeira, N. R. Colaianni, C. R. Fitzpatrick, J. L. Dangl, Beyond pathogens: microbiota interactions with the plant immune system. *Current Opinion in Microbiology* **49**, 7–17 (2019).

16. K. Yu, C. M. J. Pieterse, P. A. H. M. Bakker, R. L. Berendsen, Beneficial microbes going underground of root immunity. *Plant, Cell & Environment* **42**, 2860 (2019).

17. J. Bergelson, J. Mittelstrass, M. W. Horton, Characterizing both bacteria and fungi improves understanding of the Arabidopsis root microbiome. *Scientific Reports 2019 9:1* **9**, 1–11 (2019).

18. M. Hu, J.-M. Zhou, Research on ADR1s helps understanding the plant immune network. *Stress Biology* **2**, 12 (2022).

19. J. Bigeard, J. Colcombet, H. Hirt, Signaling mechanisms in pattern-triggered immunity (PTI). *Molecular Plant* **8**, 521–539 (2015).

20. F. Locci, J. E. Parker, Plant NLR immunity activation and execution: a biochemical perspective. *Open Biology* **14** (2024).

21. F. Monteiro, M. T. Nishimura, Structural, functional, and genomic diversity of plant NLR proteins: An evolved resource for rational engineering of plant immunity. *Annual Review of Phytopathology* **56**, 243–267 (2018).

22. G. Castrillo, P. J. P. L. Teixeira, S. H. Paredes, T. F. Law, L. De Lorenzo, M. E. Feltcher, O. M. Finkel, N. W. Breakfield, P. Mieczkowski, C. D. Jones, J. Paz-Ares, J. L. Dangl, Root microbiota drive direct integration of phosphate stress and immunity. *Nature* **543**, 513–518 (2017).

23. S. L. Lebeis, S. H. Paredes, D. S. Lundberg, N. Breakfield, J. Gehring, M. McDonald, S. Malfatti, T. G. Del Rio, C. D. Jones, S. G. Tringe, J. L. Dangl, Salicylic acid modulates colonization of the root microbiome by specific bacterial taxa. *Science* **349**, 860–864 (2015).

24. S. Pfeilmeier, G. C. Petti, M. Bortfeld-Miller, B. Daniel, C. M. Field, S. Sunagawa, J. A. Vorholt, The plant NADPH oxidase RBOHD is required for microbiota homeostasis in leaves. *Nature Microbiology* **6**, 852–864 (2021).

25. M. Frey, K. Schullehner, R. Dick, A. Fiesselmann, A. Gierl, Benzoxazinoid biosynthesis, a model for evolution of secondary metabolic pathways in plants. *Phytochemistry* **70**, 1645–1651 (2009).

26. S. Cadot, H. Guan, M. Bigalke, J. C. Walser, G. Jander, M. Erb, M. G. A. van der Heijden, K. Schlaeppi, Specific and conserved patterns of microbiota-structuring by maize benzoxazinoids in the field. *Microbiome* **9**, 1–19 (2021).

27. T. E. A. Cotton, P. Pétriacq, D. D. Cameron, M. A. Meselmani, R. Schwarzenbacher, S. A. Rolfe, J. Ton, Metabolic regulation of the maize rhizobiome by benzoxazinoids. *ISME Journal* **13**, 1647–1658 (2019).

28. S. Cadot, V. Gfeller, L. Hu, N. Singh, A. Sánchez-Vallet, G. Glauser, D. Croll, M. Erb, M. G. A. van der Heijden, K. Schlaeppi, Soil composition and plant genotype determine benzoxazinoid-mediated plant–soil feedbacks in cereals. *Plant Cell and Environment* **44**, 3502–3514 (2021).

29. V. Gfeller, J. Waelchli, S. Pfister, G. Deslandes-Hérold, F. Mascher, G. Glauser, Y. Aeby, A. Mestrot, C. A. M. Robert, K. Schlaeppi, M. Erb, Plant secondary metabolite-dependent plant-soil feedbacks can improve crop yield in the field. *eLife* **12** (2023).

30. K. Stengele, L. Stauber, L. Thoenen, H. Janse van Rensburg, V. D'Adda, K. Schlaeppi, Benzoxazinoid-mediated microbiome feedbacks enhance Arabidopsis growth and defense. bioRxiv [Preprint] (2024). https://doi.org/10.1101/2024.10.21.619081.

31. A. Martinez-Medina, V. Flors, M. Heil, B. Mauch-Mani, C. M. J. Pieterse, M. J. Pozo, J. Ton, N. M. van Dam, U. Conrath, Recognizing Plant Defense Priming. *Trends in Plant Science* **21**, 818–822 (2016).

32. P. C. A. Wintermans, P. A. H. M. Bakker, C. M. J. Pieterse, Natural genetic variation in Arabidopsis for responsiveness to plant growth-promoting rhizobacteria. *Plant Molecular Biology* **90**, 623–634 (2016).

33. The 1001 Genomes Consortium, 1,135 Genomes Reveal the Global Pattern of Polymorphism in Arabidopsis thaliana. *Cell* **166**, 481–491 (2016).

34. P. Hüther, N. Schandry, K. Jandrasits, I. Bezrukov, C. Becker, ARADEEPOPSIS, an automated workflow for top-view plant phenomics using semantic segmentation of leaf States. *Plant Cell* **32**, 3674–3688 (2020).

35. R. G. Belz, K. Hurle, Differential exudation of two benzoxazinoids - One of the determining factors for seedling allelopathy of Triticeae species. *Journal of Agricultural and Food Chemistry* **53**, 250–261 (2005).

36. N. Schandry, C. Becker, Allelopathic Plants: Models for Studying Plant–Interkingdom Interactions. *Trends in Plant Science* **25**, 176–185 (2020).

37. V. Gfeller, S. Cadot, J. Waelchli, S. Gulliver, C. Terrettaz, L. Thönen, P. Mateo, C. A. M. Robert, F. Mascher, T. Steinger, M. Bigalke, M. Erb, K. Schlaeppi, Soil chemical and microbial gradients determine accumulation of root-exuded secondary metabolites and plant–soil feedbacks in the field. *Journal of Sustainable Agriculture and Environment* **2**, 173–188 (2023).

38. C. Lippert, F. P. Casale, B. Rakitsch, O. Stegle, LIMIX: genetic analysis of multiple traits. doi: 10.1101/003905 (2014).

39. J. A. Dongus, J. E. Parker, EDS1 signalling: At the nexus of intracellular and surface receptor immunity. *Current Opinion in Plant Biology* **62**, 102039 (2021).

40. J. Ordon, J. Gantner, J. Kemna, L. Schwalgun, M. Reschke, J. Streubel, J. Boch, J. Stuttmann, Generation of chromosomal deletions in dicotyledonous plants employing a user-friendly genome editing toolkit. *Plant Journal* **89**, 155–168 (2017).

41. R. N. Pruitt, F. Locci, F. Wanke, L. Zhang, S. C. Saile, A. Joe, D. Karelina, C. Hua, K. Fröhlich, W. L. Wan, M. Hu, S. Rao, S. C. Stolze, A. Harzen, A. A. Gust, K. Harter, M. H. A. J. Joosten, B. P. H. J. Thomma, J. M. Zhou, J. L. Dangl, D. Weigel, H. Nakagami, C. Oecking, F. E. Kasmi, J. E. Parker, T. Nürnberger, The EDS1–PAD4–ADR1 node mediates Arabidopsis pattern-triggered immunity. *Nature* **598**, 495–499 (2021).

42. J. Lang, B. Genot, J. Bigeard, J. Colcombet, MPK3 and MPK6 control salicylic acid signaling by up-regulating *NLR* receptors during pattern- and effector-triggered immunity. *Journal of Experimental Botany* **73**, 2190–2205 (2022).

43. T. Chen, K. Nomura, X. Wang, R. Sohrabi, J. Xu, L. Yao, B. C. Paasch, L. Ma, J. Kremer, Y. Cheng, L. Zhang, N. Wang, E. Wang, X. F. Xin, S. Y. He, A plant genetic network for preventing dysbiosis in the phyllosphere. *Nature* **580**, 653–657 (2020).

44. P. Runge, "Structural variation of a polymorphic RPP1-like cluster in local Arabidopsis thaliana populations alters phyllosphere microbiome in Gorzów Wielkopolski," thesis, University of Tübingen, Germany (2022).

45. S. Goritschnig, A. D. Steinbrenner, D. J. Grunwald, B. J. Staskawicz, Structurally distinct Arabidopsis thaliana NLR immune receptors recognize tandem WY domains of an oomycete effector. *New Phytologist* **210**, 984–996 (2016).

46. D. Maag, A. Köhler, C. A. M. Robert, M. Frey, J. L. Wolfender, T. C. J. Turlings, G. Glauser, M. Erb, Highly localized and persistent induction of Bx1-dependent herbivore resistance factors in maize. *The Plant Journal* **88**, 976–991 (2016).

47. D. Jirage, T. L. Tootle, T. L. Reuber, L. N. Frost, B. J. Feys, J. E. Parker, F. M. Ausubel, J. Glazebrook, Arabidopsis thaliana PAD4 encodes a lipase-like gene that is important for salicylic acid signaling. *Proceedings of the National Academy of Sciences* **96**, 13583–13588 (1999).

48. X. Sun, D. Lapin, J. M. Feehan, S. C. Stolze, K. Kramer, J. A. Dongus, J. Rzemieniewski, S. Blanvillain-Baufumé, A. Harzen, J. Bautor, P. Derbyshire, F. L. H. Menke, I. Finkemeier, H. Nakagami, J. D. G. Jones, J. E. Parker, Pathogen effector recognition-dependent association of NRG1 with EDS1 and SAG101 in TNL receptor immunity. *Nat Commun* **12**, 3335 (2021).

49. C. Cardoso, T. Charnikhova, M. Jamil, P. M. Delaux, F. Verstappen, M. Amini, D. Lauressergues, C. Ruyter-Spira, H. Bouwmeester, Differential activity of Striga hermonthica seed germination stimulants and Gigaspora rosea hyphal branching factors in rice and their contribution to underground communication. *PLoS ONE* **9** (2014).

50. M. Togninalli, Ü. Seren, D. Meng, J. Fitz, M. Nordborg, D. Weigel, K. Borgwardt, A. Korte, D. G. Grimm, The AraGWAS Catalog: A curated and standardized Arabidopsis thaliana GWAS catalog. *Nucleic Acids Research* **46**, D1150–D1156 (2018).

51. Á. Ferrero-Serrano, S. M. Assmann, Phenotypic and genome-wide association with the local environment of Arabidopsis. *Nature Ecology and Evolution* **3**, 274–285 (2019).

52. E. Knoch, J. Kovács, S. Deiber, R. Shanmuganathan, N. Serra Serra, C. Becker, N. Schandry, N. Serra, S. C. Becker, Transcriptional response of a target plant to benzoxazinoid and diterpene allelochemicals highlights commonalities in detoxification. *bioRxiv*, 2022.02.21.480921 (2022).

53. C. A. Schneider, W. S. Rasband, K. W. Eliceiri, NIH Image to ImageJ: 25 years of Image Analysis. *Nat Methods* **9**, 671–675 (2012).

54. D. S. Lundberg, P. P. N. Ayutthaya, A. Strauß, G. Shirsekar, W. S. Lo, T. Lahaye, D. Weigel, Host-associated microbe pcr (Hampcr) enables convenient measurement of both microbial load and community composition. *eLife* **10** (2021).

55. Y. Bai, D. B. Müller, G. Srinivas, R. Garrido-Oter, E. Potthoff, M. Rott, N. Dombrowski, P. C. Münch, S. Spaepen, M. Remus-Emsermann, B. Hüttel, A. C. McHardy, J. A. Vorholt, P. Schulze-Lefert, Functional overlap of the Arabidopsis leaf and root microbiota. *Nature 2015 528:7582* **528**, 364–369 (2015).

56. K. L. McGuire, S. G. Payne, M. I. Palmer, C. M. Gillikin, D. Keefe, S. J. Kim, S. M. Gedallovich, J. Discenza, R. Rangamannar, J. A. Koshner, A. L. Massmann, G. Orazi, A. Essene, J. W. Leff, N. Fierer, Digging the New York City Skyline: Soil Fungal Communities in Green Roofs and City Parks. *PLOS ONE* **8**, e58020 (2013).

57. M. Martin, Cutadapt removes adapter sequences from high-throughput sequencing reads. *EMBnet.journal* **17**, 10 (2011).

58. B. J. Callahan, P. J. McMurdie, M. J. Rosen, A. W. Han, A. J. A. Johnson, S. P. Holmes, DADA2: High-resolution sample inference from Illumina amplicon data. *Nature Methods* **13**, 581–583 (2016).

59. C. Quast, E. Pruesse, P. Yilmaz, J. Gerken, T. Schweer, P. Yarza, J. Peplies, F. O. Glöckner, The SILVA ribosomal RNA gene database project: Improved data processing and web-based tools. *Nucleic Acids Research* **41**, D590 (2013).

60. E. S. Wright, Using DECIPHER v2.0 to analyze big biological sequence data in R. *R Journal* **8**, 352–359 (2016).

61. J. Oksanen, G. L. Simpson, F. G. Blanchet, R. Kindt, P. Legendre, P. R. Minchin, R. B. O'Hara, P. Solymos, M. H. H. Stevens, E. Szoecs, H. Wagner, M. Barbour, M. Bedward, B. Bolker, D. Borcard, G. Carvalho, M. Chirico, M. D. Caceres, S. Durand, H. B. A. Evangelista, R. FitzJohn, M. Friendly, B. Furneaux, G. Hannigan, M. O. Hill, L. Lahti, D. McGlinn, M.-H. Ouellette, E. R. Cunha, T. Smith, A. Stier, C. J. F. T. Braak, J. Weedon, vegan: Community Ecology Package, version 2.6-6.1 (2024); https://cran.r-project.org/web/packages/vegan/index.html.

62. S. Weiss, Z. Z. Xu, S. Peddada, A. Amir, K. Bittinger, A. Gonzalez, C. Lozupone, J. R. Zaneveld, Y. Vázquez-Baeza, A. Birmingham, E. R. Hyde, R. Knight, Normalization and microbial differential abundance strategies depend upon data characteristics. *Microbiome* **5**, 1–18 (2017).

852 63. E. Montassier, G. A. Al-Ghalith, B. Hillmann, K. Viskocil, A. J. Kabage, C. E.
853 McKinlay, M. J. Sadowsky, A. Khoruts, D. Knights, CLOUD: A non-parametric
854 detection test for microbiome outliers. *Microbiome* **6**, 1–10 (2018).

855 64. P. J. McMurdie, S. Holmes, phyloseq: an R package for reproducible interactive
856 analysis and graphics of microbiome census data. *PLoS One* **8**, e61217 (2013).

857 65. A. Dobin, C. A. Davis, F. Schlesinger, J. Drenkow, C. Zaleski, S. Jha, P. Batut, M.
858 Chaisson, T. R. Gingeras, STAR: ultrafast universal RNA-seq aligner. *Bioinformatics*
859 **29**, 15–21 (2013).

860 66. M. I. Love, W. Huber, S. Anders, Moderated estimation of fold change and dispersion
861 for RNA-seq data with DESeq2. *Genome Biology* **15**, 550 (2014).

862 67. A. Rau, C. Maugis-Rabusseau, Transformation and model choice for RNA-seq co-
863 expression analysis. *Briefings in Bioinformatics* **19**, 425–436 (2018).

864 68. M. Kolmogorov, J. Yuan, Y. Lin, P. A. Pevzner, Assembly of long, error-prone reads
865 using repeat graphs. *Nat Biotechnol* **37**, 540–546 (2019).

866 69. M. Naish, M. Alonge, P. Wlodzimierz, A. J. Tock, B. W. Abramson, A. Schmücker, T.
867 Mandáková, B. Jamge, C. Lambing, P. Kuo, N. Yelina, N. Hartwick, K. Colt, L. M.
868 Smith, J. Ton, T. Kakutani, R. A. Martienssen, K. Schneeberger, M. A. Lysak, F.
869 Berger, A. Bousios, T. P. Michael, M. C. Schatz, I. R. Henderson, The genetic and
870 epigenetic landscape of the Arabidopsis centromeres. *Science* **374**, eabi7489 (2021).

871 70. M. Alonge, L. Lebeigle, M. Kirsche, K. Jenike, S. Ou, S. Aganezov, X. Wang, Z. B.
872 Lippman, M. C. Schatz, S. Soyk, Automated assembly scaffolding using RagTag
873 elevates a new tomato system for high-throughput genome editing. *Genome Biology* **23**,
874 258 (2022).

875 71. A. Shumate, S. L. Salzberg, Liftoff: accurate mapping of gene annotations.
876 *Bioinformatics* **37**, 1639–1643 (2021).

877

878

Supplementary Materials

Title:

A TNL receptor mediates microbiome feedbacks in Arabidopsis

Authors:

Henry Janse van Rensburg[1*], Niklas Schandry[2,3*§], Jan Waelchli[1], Katja Stengele[1], Selma Cadot[1], Katharina Jandrasits[2], Claude Becker[2,3,§], Klaus Schlaeppi[1,§]

[1] Department of Environmental Sciences, University of Basel, Basel, Switzerland

[2] Gregor Mendel Institute of Molecular Plant Biology GmbH, Austrian Academy of Sciences, Vienna BioCenter (VBC), Vienna, Austria

[3] LMU Biocenter, Faculty of Biology, Ludwig-Maximilians-Universität Munich, Martinsried, Germany

The file includes:

Figures S1 to S9

Tables S1 to S3

Other Supplementary Materials for this manuscript include

Dataset S1 to S6 (Input data to reproduce figures)

Supplementary Files 1 to 6 (R markdown files to reproduce analysis)

Supplementary Figures

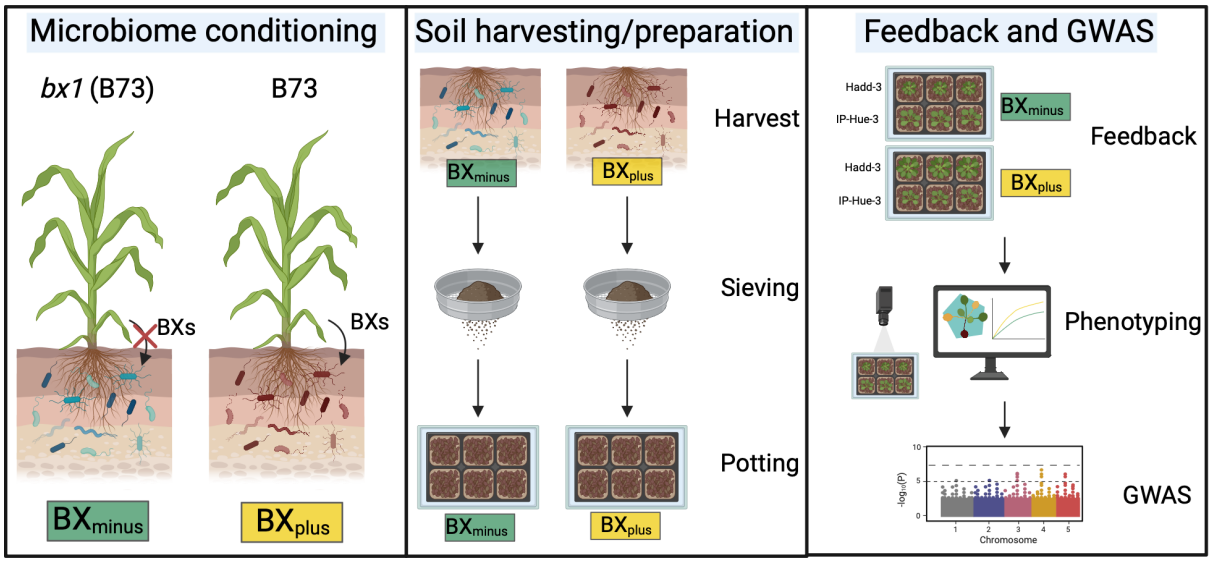

Figure S1. **Overview of the experimental workflow**. To condition the soil microbiomes, maize exuding BXs (B73) and a BX-deficient mutant (*bx1*) was grown for 12 weeks on field soil, resulting in a BX_{plus} and a BX_{minus} microbiome. The soil core surrounding the roots was removed and sieved to produce the soil used for growth-feedback assays. 410 Arabidopsis accessions were grown on the two conditioned soil microbiomes and phenotyped using a high-throughput phenotyping pipeline. Growth feedback response as the rosette size (BX_{plus} – BX_{minus}) on the two soil microbiomes was used as the phenotype for the genome-wide association study (GWAS). *Mediator of microbiome feedbacks 1* (*MMF1*) identified in the GWAS was functionally validated for growth feedback assays using T-DNA insertion mutant lines. The cause for lack of feedback in mutants were further dissected by analysing the microbiome and transcriptome of wild-type and mutant plants grown on the two microbiomes. Created with BioRender®.

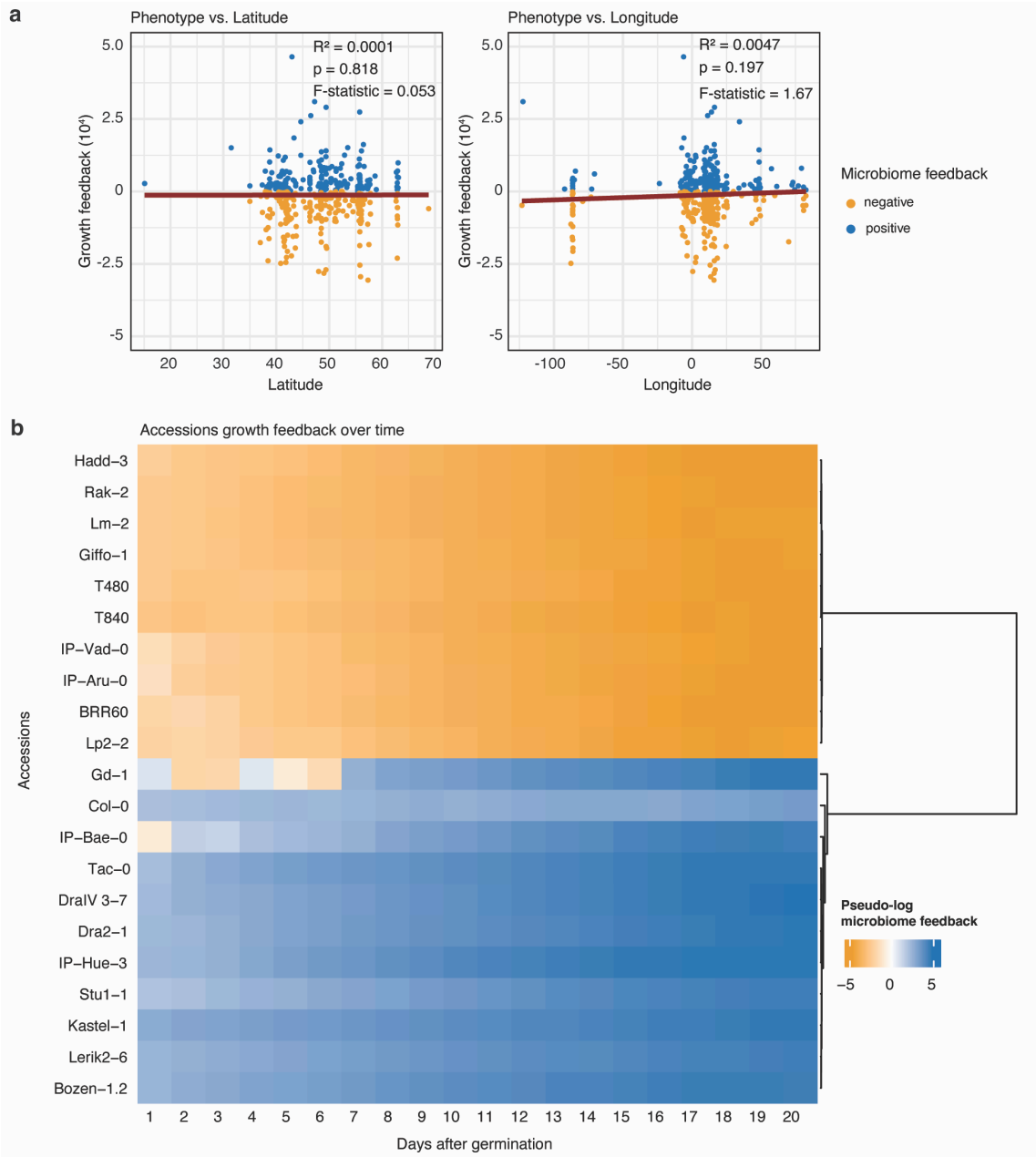

Figure S2. **Microbiome feedback of Arabidopsis accessions**. (**a**) Relationship between growth feedbacks and geographical location of the phenotyped accessions. Scatter plot illustrating the relationship between latitude or longitude and the microbiome feedback of accessions at 15 days after germination. Each data point is coloured according to its microbiome feedback response, with orange and blue denoting a negative or positive microbiome feedback, respectively. The plot includes a linear regression line (in red), highlighting the relationship between location and phenotype. The regression statistics, including the R-squared value (R^2) and the *p*-value of the F-test, are displayed in the top right corner of the plot. The R-squared value quantifies the proportion of variance in the phenotype explained by either latitude or longitude, while the *p*-value refers to testing the null hypothesis that the slope of the regression line is zero. (**b**) The daily microbiome feedback of Col-0 and the top 10 accessions with the strongest positive (blue) or negative (orange) BX-growth feedback when grown on the BX_{plus} and BX_{minus} soils. The heatmap colours are the pseudo-log transformed microbiome feedbacks (rosette area on BX_{plus} – rosette area on BX_{minus}). Accessions are clustered on the y-axis based on agglomerative hierarchical clustering using Ward's method performed using Dynamic Time Warping (DTW) distances and Ward's method to identify groups with similar response patterns over time. The dendrogram on the right side of the heat map illustrates the clustering structure, grouping accessions that exhibit similar trajectories in their growth feedback **Dataset 1**.

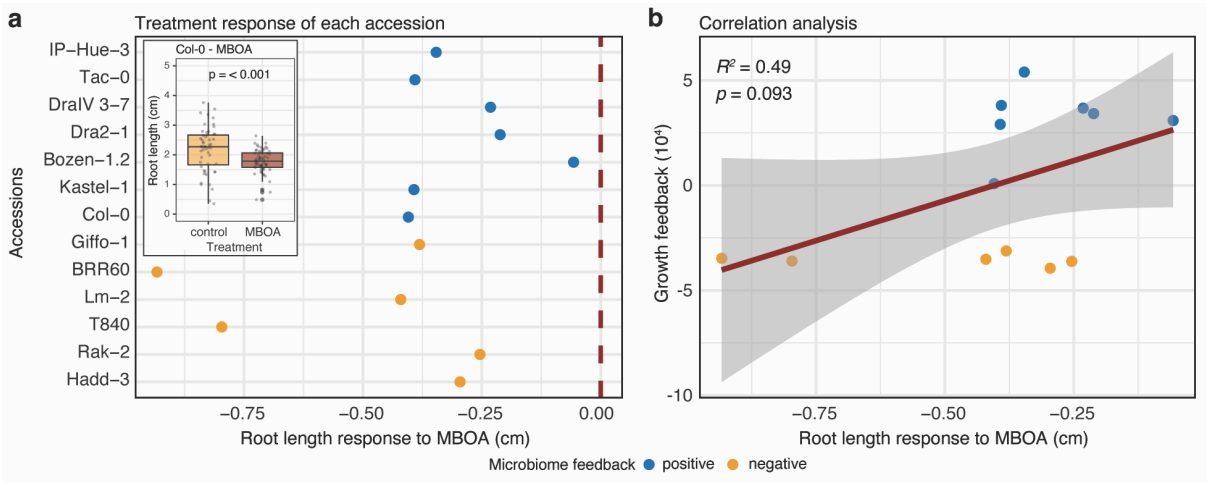

Figure S3. Direct allelopathic effect of benzoxazinoids on the growth of Arabidopsis. (**a**) Sensitivity to MBOA in terms of root length response (root length on control – root length on MBOA) of Col-0 and the accessions with the strongest positive or negative microbiome feedback. Accessions are colour-coded as to whether they showed a positive (blue) or negative (orange) microbiome feedback on the BX-conditioned soil microbiome in the GWAS experiment. Boxplot insert displays the root length of Col-0 on the control or MBOA treatment as an example. Plants were grown for 10 days on ½ MS media in the presence of 0.25 mM MBOA or control (DMSO). (**b**) Pearson's correlation analysis between MBOA sensitivity and microbiome feedback at 15 days after germination across the different accessions. The scatter plot displays individual data points coloured by microbiome feedback, with positive responses shown in blue and negative responses in orange. A linear regression line (in red) illustrates the trend between the two variables. The correlation coefficient (R^2) and p-value are annotated on the plot, indicating the strength and statistical probability of the relationship. **Dataset 2.**

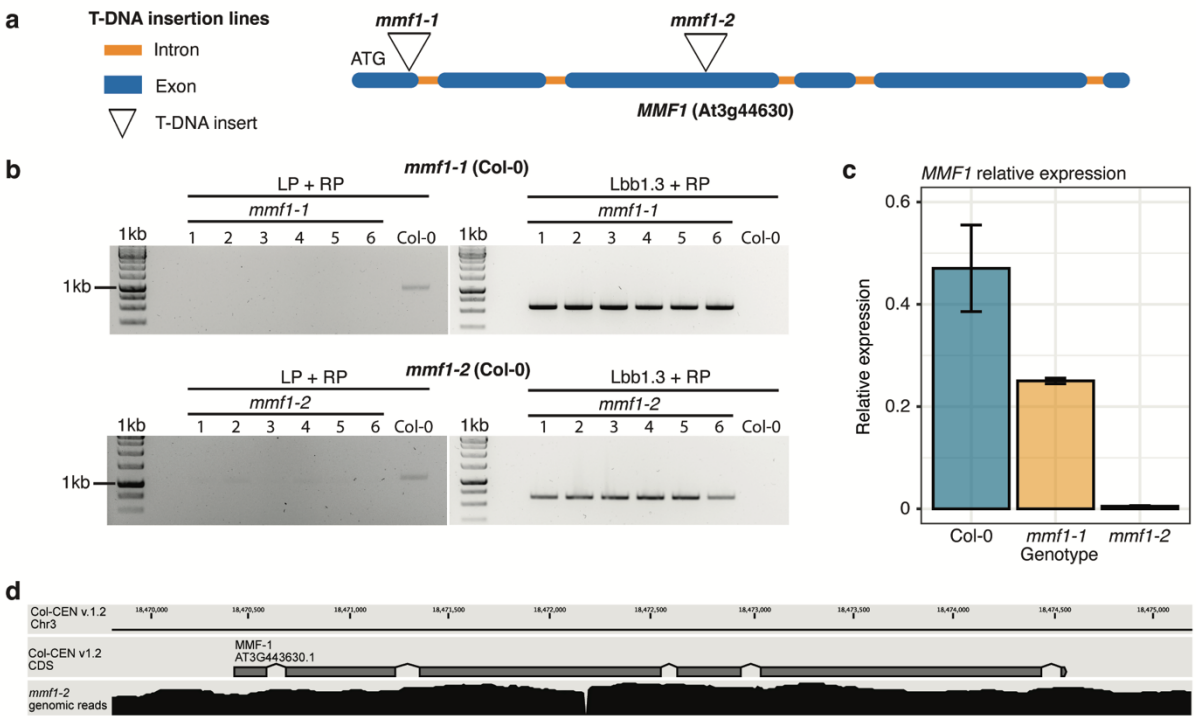

Figure S4. **Genetic characterization of *mmf1* T-DNA insertion lines.** (**a**) Genomic location of the T-DNA insertion sites for *mmf1-1* and *mmf1-2* in the open reading frame of *MMF1*. Exons and introns are shown in colour, and the T-DNA insertion position as triangles. (**b**) Genotyping results of *mmf1-1* (SALK_144159C) and *mmf1-2* (SALK_002318C) by PCR to confirm the presence of the T-DNA insertion. The gels represent genotyping of 6 mutant plants for the T-DNA insertion allele (left, LBb1.3 and RP primers) and the wild-type allele (right, LP and RP primers). (**c**) Relative expression levels of *MMF1* determined by qRT-PCR in wild-type (Col-0) and the two *MMF1* mutant lines. (**d**) Mapping of genomic long-reads from *mmf1-2* onto Col-CEN v1.2. Top panel shows the genomic coordinates on chromosome 3, middle panel shows the annotation of the coding sequence of *mmf-1,* bottom panel shows the aggregated pile-up of mapped reads, confirming the T-DNA insertion in the third exon.

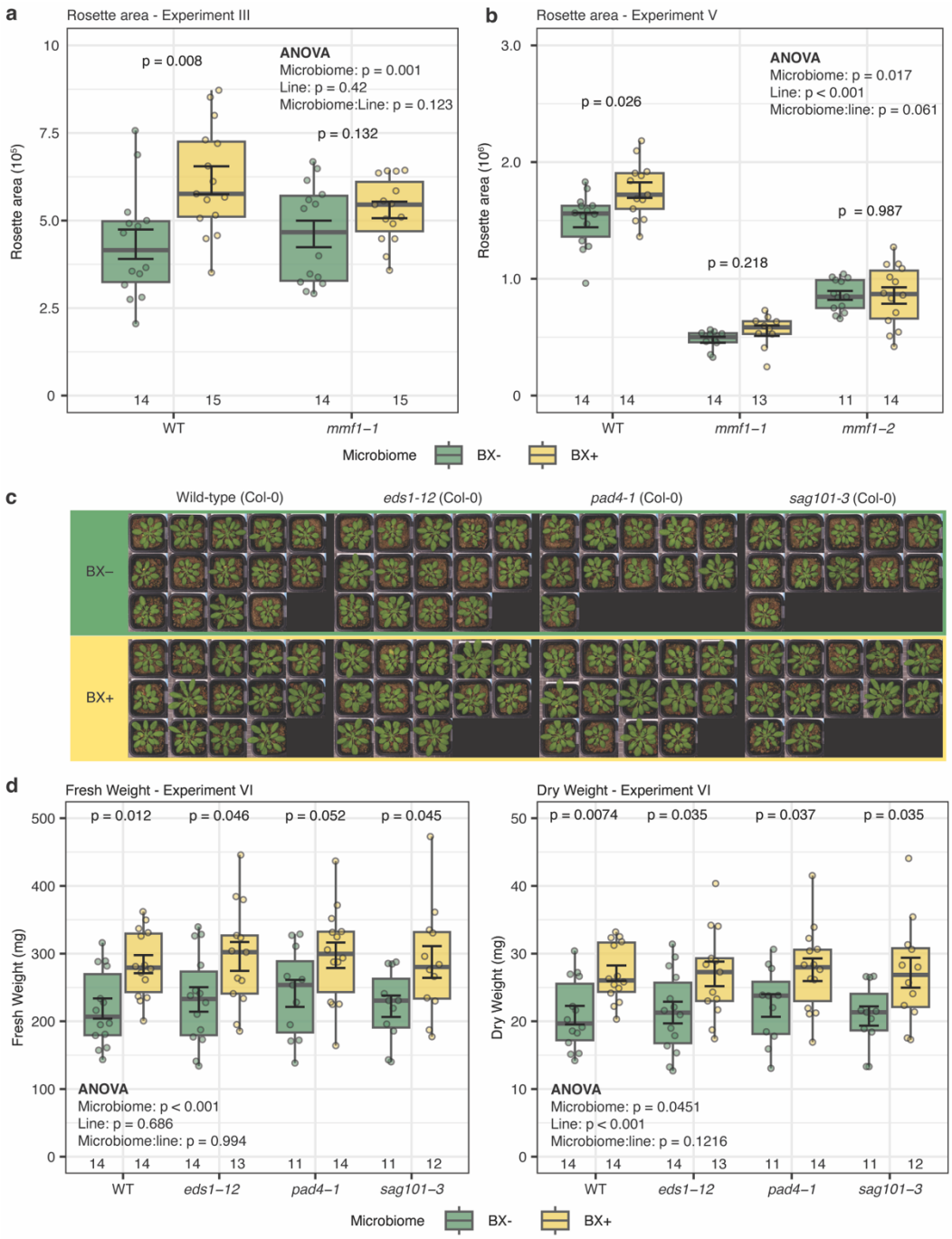

Figure S5. **Growth feedback in a BX_{plus} microbiome remains intact in effector-triggered immunity signalling mutants.** (**a** and **b**) Repeated growth feedbacks (Experiment II and IV) of Col-0 wild-type (WT) and two *mmf1* T-DNA insertion mutants (*At3g44630*) grown on the BX_{minus} and BX_{plus} soil microbiomes. Feedback experiments were performed on greenhouse-conditioned soil batches (**a**) BS04 and (**b**) BS09. Graphs illustrate the rosette area (in pixels) of 6-week-old plants. Sample sizes are indicated at the bottom of each plot. Output of the ANOVA and FDR corrected *p*-values are indicated in each plot. (**c**) Phenotypes of 6-week-old WT, and mutants (*eds1-12*, *pad4-1* and *sag101-3*) affected in effector-triggered immunity signalling pathways grown on the BX_{minus} and BX_{plus} soils. (**b**) Fresh weight, and dry weight of WT, *eds1-12*, *pad4-1* and *sag101-3* illustrate the positive growth feedback on the BX_{plus} soil microbiome. Boxplots illustrate the median, standard error, and interquartile range, and the whiskers extend from the box to the smallest and largest values. Sample numbers are indicated at the bottom of each plot. ANOVA output and FDR-corrected *p*-values comparing the growth feedback of each line are shown above the graph. **Dataset 4.**

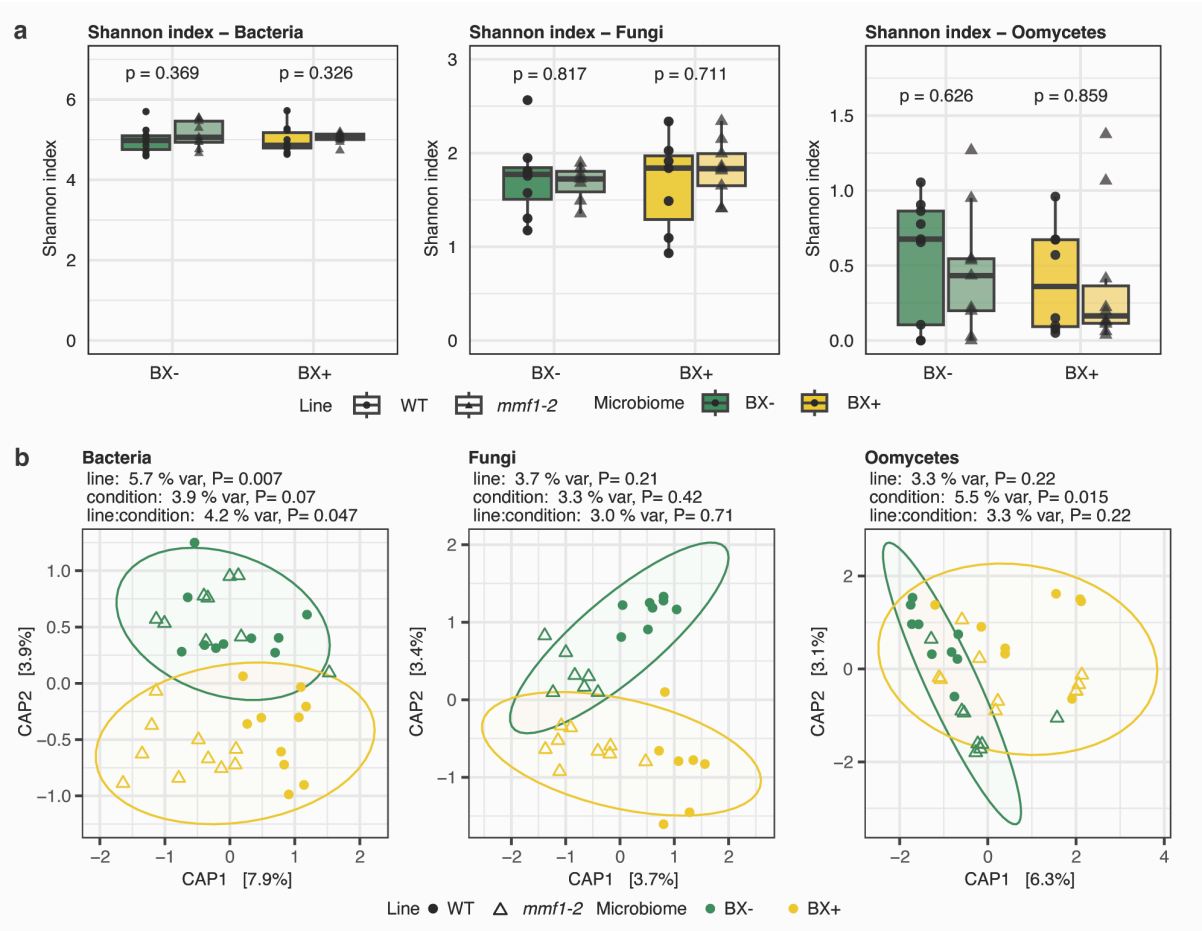

Figure S6. **Root microbiota profiling of WT and *mmf1-2* mutants grown on the BX_{minus} or BX_{minus} soils**. (**a**) Bacterial, fungal and oomycete richness in the roots of wild-type (WT) and *mmf1-2* mutants grown on BX_{plus} and BX_{minus} soil displayed as Shannon indices. Individual samples are shown as dots. Comparisons between the two lines are shown as *p*-values based on Kruskal-Wallis Test. (**b**) The output of PERMANOVA on Bray-Curtis dissimilarities of the bacterial, fungal and oomycete root microbiota of Arabidopsis WT (filled circles) and *mmf1-2* mutants (open triangles) grown on the BX_{minus} (green) and BX_{plus} (yellow) soils. The R^2 and *p* values indicate the line and conditioning effect and their interaction on the two soils. Constrained Analysis of Principal Coordinates (CAP) visually illustrating the effects found in the PERMANOVA analysis. Plants grown on a BX_{plus} (yellow) and BX_{minus} (green) soil microbiome are grouped based on a 95% confidence interval. The axes show the percentage of explained variance for the first two principal components.

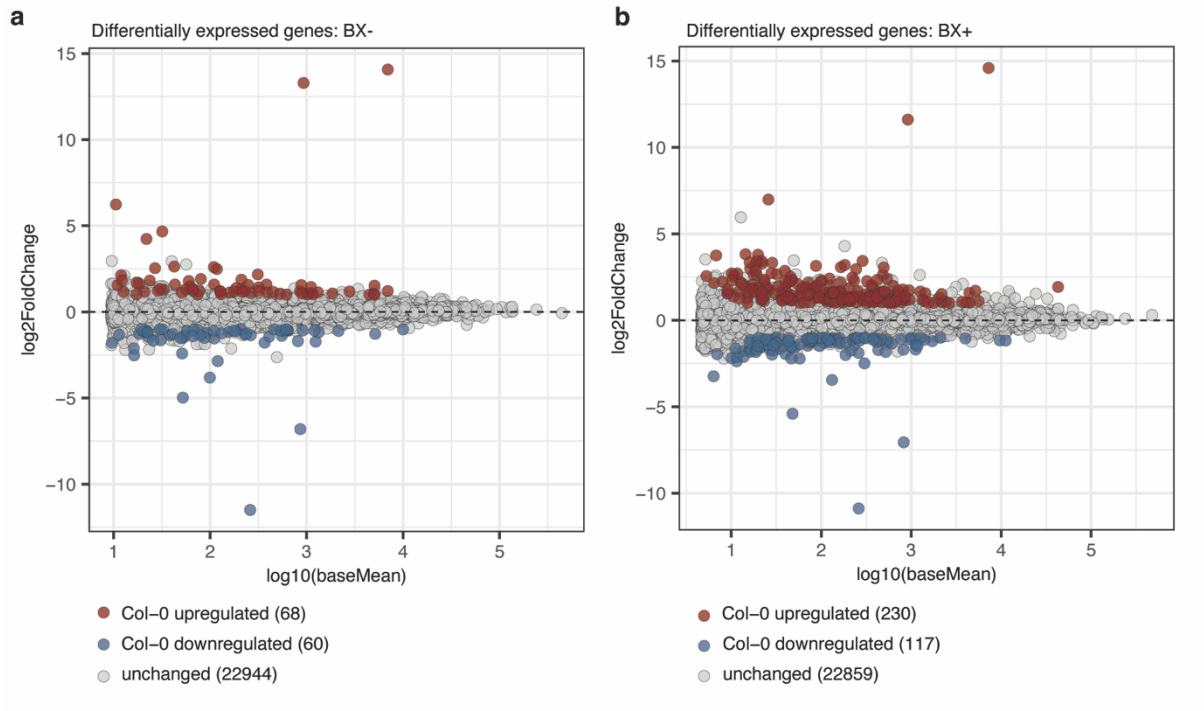

991
992 **Figure S7**. **Root transcriptome of WT and *mmf1-2* mutants grown on the BX_{minus} and BX_{plus} soils.** MA plot
993 of differentially expressed genes between *mmf1-2* mutants and WT plants in response to the (**a**) BX_{minus} and (**b**)
994 BX_{plus} soil microbiome. Significantly differentially expressed genes were calculated using DESeq2 (log_2fold
995 change ≥ 1; empirical Bayes statistic false discovery rate < 0.05).
996

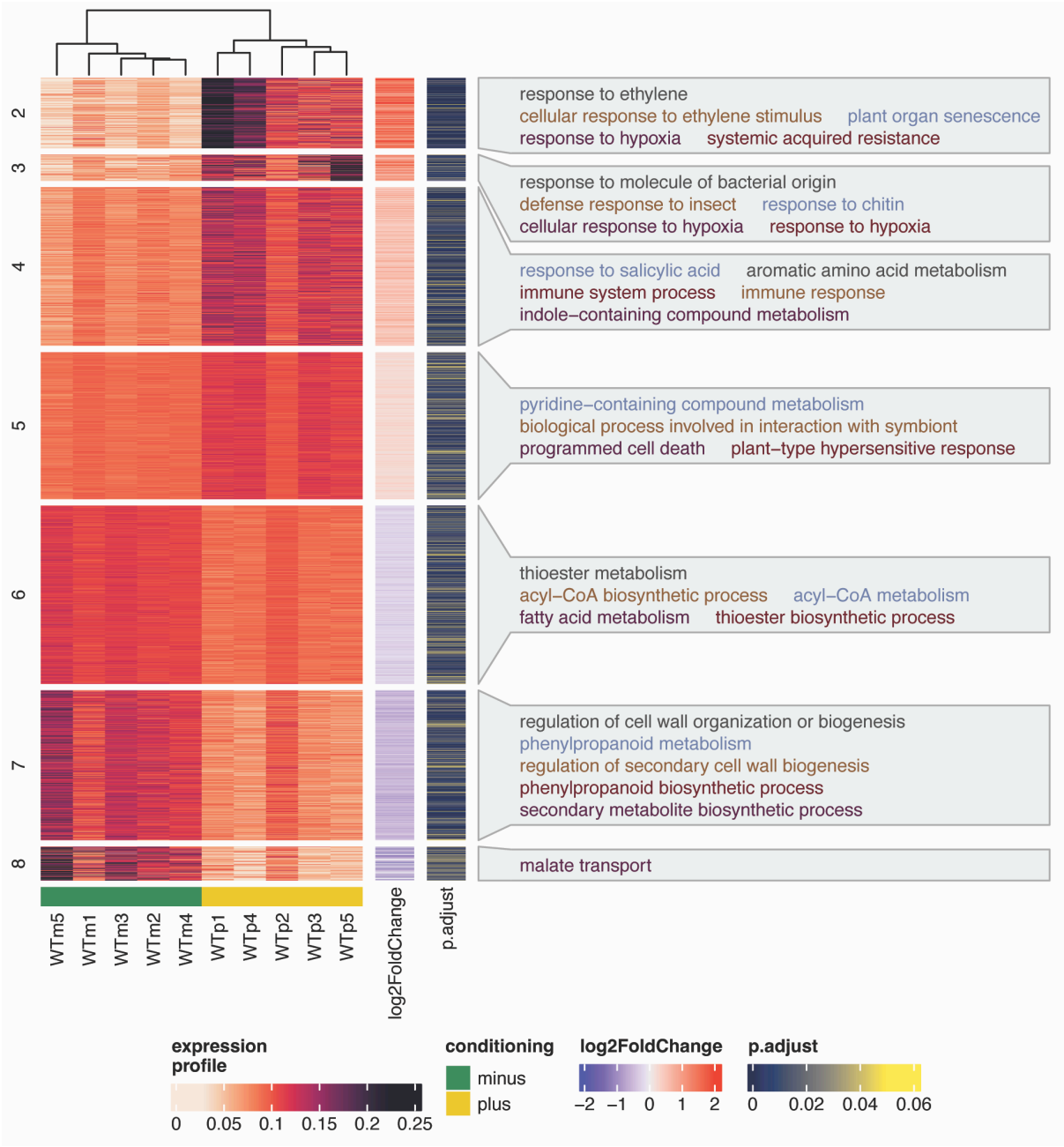

Figure S8. **Heatmap illustrating the co-expression analysis of the Arabidopsis WT root transcriptome grown on the BX_{minus} and BX_{plus} soil microbiome.** Heatmap showing the co-expressed gene clusters (Benjamini-Hochberg-correction, p-adjust < 0.01) as identified by coseq for plants grown on BX_{minus} (green) or BX_{plus} (yellow) soils. Colours of the heatmap indicates the expression profiles in terms of normalized gene counts for each gene. The log2Fold change and adjusted *p* values (empirical Bayes shrinking) for each gene inferred from DESeq2 is shown on the right. Cluster labels show the top 5 enriched GO terms for biological function within each cluster. GO text colour is for better readability only. Full tables of all enriched GO terms in each cluster are provided in **Dataset 6**.

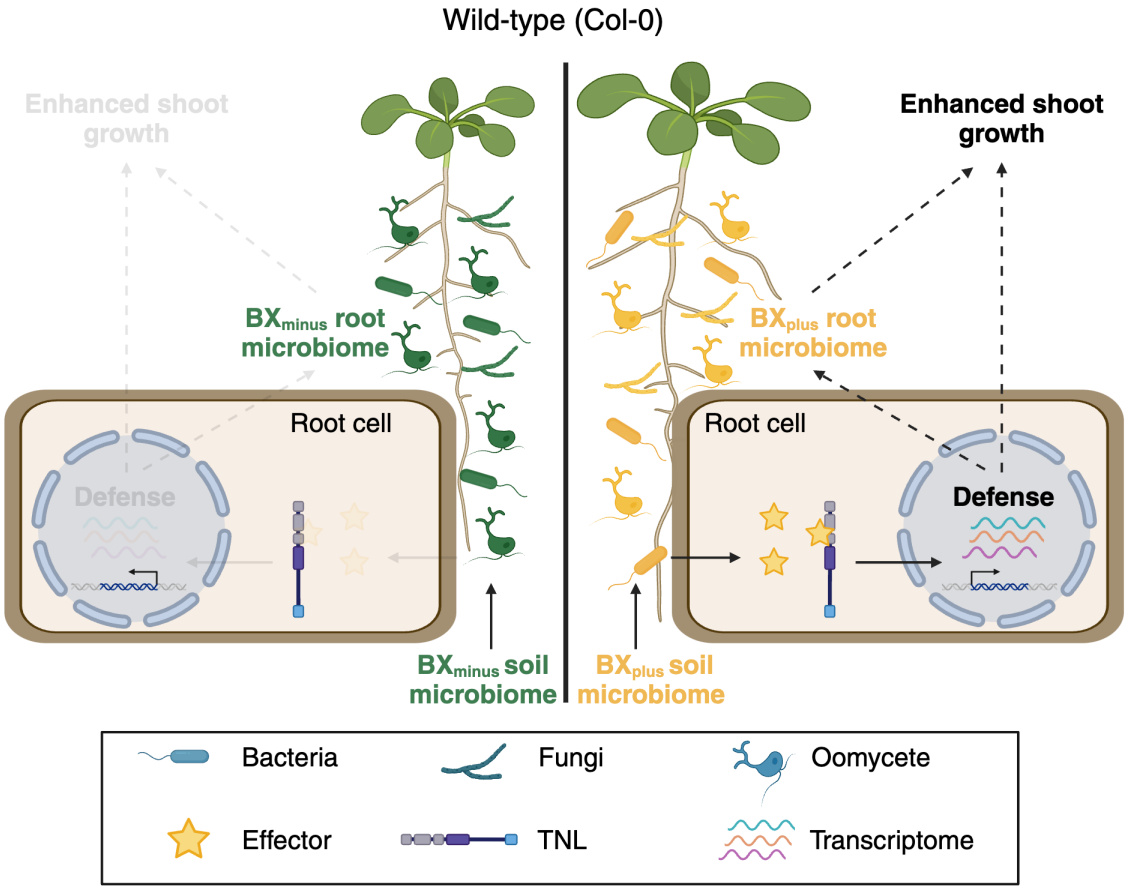

Figure S9. **Proposed model of microbiome feedbacks through MMF1 in Col-0 plants**. Plants with a functional MMF1 receptor perceive a putative effector molecule that is present in the BX_{plus} soil microbiome, mounting a defence response that coincides with an altered root microbiome and promoted plant growth. The absence of this effector molecule in the BX_{minus} microbiome results in the lack of defence responses in plants grown on this soil microbiome. Col-0 plants lacking the MMF1 receptor fail to perceive the effector molecule from the BX_{plus} microbiome and do not mount defence responses; they have a different microbiome, and no enhanced shoot growth is observed. Figure created with BioRender®.

Supplementary Tables

Table S1: Setup and growth conditions of the different experiments performed in this study. For each of the microbiome feedback experiments in the manuscript, the soil batch, measurement in terms of data generated, and time from start to conclusion is indicated.

Experiment	Plants	Soil batch	Measurement	Growth (weeks)
Exp. I	Accessions run 1	1	Growth (210 accessions)	12
Exp. II	Accessions run 2	2	Growth (210 accessions)	9
Exp. III	*mmf1* rep. 1	3	Growth	6
Exp. IV	*mmf1* rep. 2	3	Growth, microbiota, transcriptome	6
Exp. V	*mmf1* rep. 3	4	Growth	6
Exp. VI	ETI mutants	4	Growth	6

Table S2: **Set up of the different microbiome conditioning experiments**. Each "soil batch" denotes an independent conditioning experiment from soils collected from three adjacent Agroscope research fields in Changins, Nyon, Switzerland (46°24'00.0"N, 6°14'22.8"E). The "scollection" column specifies when and from which field (Parcel) the soil was collected. For fertilization in the greenhouse, pots were treated weekly with the indicated solution. Abbreviations: "rel. hum." = relative humidity; "int." = intensity.

Soil batch	Collection	Conditioning	Fertilization	Growth conditions
Batch 1	April 2018 (Parcel 30/31)	Field[1]	NA[3]	Conventional farming
Batch 2	Dec. 2019 (Parcel 30/31)	Field[1]	NA[3]	Conventional farming
Batch 3	Aug. 2020 (Parcel 30/31)	Greenhouse	4 w. low iron,[4] 8 w. high iron[5]	16 h day at min. 23°C, 8 h night at min. 19°C, >500 µmol m^{-2} s^{-1} light int.
Batch 4	Sept. 2022 (Parcel 29/30)	Phytotron[2]	12 w. low iron[4]	14 h day at 22°C, 10 h night at 18°C, 60% rel. hum., ~550 µmol m^{-2} s^{-1} light int.

[1]Soil conditioning was performed in the field, and soil cores harvested at the conclusion (collection) of the conditioning.
[2]Phytotron Facility, University of Basel, Switzerland
[3]Fields were managed according to conventional Swiss farming practices, including the use of agrochemicals.
[4]100 mL of 0.2% Plantaaktiv Typ K (Hauert HBG Duenger AG, Grossaffoltern, Switzerland) and 0.0001% Sequestrene Rapid (Maag, Westland Schweiz GmbH, Dielsdorf, Switzerland)
[5]200 mL of 0.2% Plantaaktiv Typ K, 0.02% Sequestrene Rapid.

1044 **Table S3: Primer names and sequences used in this study**

Primer name	Purpose	Primer sequence
***mmf1-1*_LP**	Genotyping	GAAGGCTTTTCCAAATTCACC
***mmf1-2*_RP**	Genotyping	ACCAAAATTCCATTAAACCCG
***mmf1-2*_LP**	Genotyping	TAAGGATAATCGGGATTTGGG
***mmf1-2*_RP**	Genotyping	TCCTGAAACATGAGCCAAAAG
LBb1.3	Genotyping	ATTTTGCCGATTTCGGAAC
***mmf1*_Fw**	*qPCR*	TCGCATGTGAGGCATACGAA
***mmf1*_Rev**	*qPCR*	GCGGTGATGAACGAATTGCT
PP2A_Fw	*qPCR*	CCTGCGGTAATAACTGCATCT
PP2A_Rev	*qPCR*	CTTCACTTAGCTCCACCAAGCA
CS1-*fs*-799-F	Microbiome	ACACTGACGACATGGTTCTACA*fs*AACMGGATTAGATACCCKG
CS2-*fs*-1193R	Microbiome	TACGGTAGCAGAGACTTGGTCT*fs*ACGTCATCCCCACCTTCC
CS1-At.GI-F	Microbiome	ACACTGACGACATGGTTCTACACTGTAAAGATAAATGGGTCATCTAA
CS2-At-GI-R	Microbiome	TACGGTAGCAGAGACTTGGTCTAAGGGTTCAGCTTTGTCAACAA
ITS1-F	Microbiome	ACACTGACGACATGGTTCTACACTTGGTCATTTAGAGGAAGTAA
ITS2-R	Microbiome	TACGGTAGCAGAGACTTGGTCTGCTGCGTTCTTCATCGATGC
ITS1-O_F1_G-46636	Microbiome	ACACTGACGACATGGTTCTACACGGAAGGATCATTACCAC
5.8s-O_R1_G-46637	Microbiome	TACGGTAGCAGAGACTTGGTCTAGCCTAGACATCCACTGCTG

1045
1046
1047